DISCLAIMER

This report was prepared as an account of work sponsored by an agency of the United States Government. Neither the United States Government nor any agency thereof, nor any of their employees, makes any warranty, express or implied, or assumes any legal liability or responsibility for the accuracy, completeness, or usefulness of any information, apparatus, product, or process disclosed, or represents that its use would not infringe privately owned rights. Reference herein to any specific commercial product, process, or service by trade name, trademark, manufacturer, or otherwise does not necessarily constitute or imply its endorsement, recommendation, or favoring by the United States Government or any agency thereof. The views and opinions of authors expressed herein do not necessarily state or reflect those of the United States Government or any agency thereof. Reference herein to any social initiative (including but not limited to Diversity, Equity, and Inclusion (DEI); Community Benefits Plans (CBP); Justice 40; etc.) is made by the Author independent of any current requirement by the United States Government and does not constitute or imply endorsement, recommendation, or support by the United States Government or any agency thereof.

ANL/RAS 88-6

RADIAL CORE EXPANSION REACTIVITY FEEDBACK: CURRENT UNDERSTANDING AND THE SASSYS/SAS4A MODEL

by

R. A. Wigeland

September 1988

~~APPLIED TECHNOLOGY~~

~~Any further distribution by any holder of this document or data therein to third parties representing foreign interests, foreign governments, foreign companies, and foreign subsidiaries or foreign divisions of U. S. companies shall be approved by the Associate Deputy Assistant Secretary for Reactor Systems, Development, and Technology, U. S. Department of Energy. Further, foreign party release may require DOE approval pursuant to Federal Regulation 10 CFR Part 810, and/or may be subject to Section 127 of the Atomic Energy Act.~~

~~NOTICE: This informal document contains preliminary information prepared primarily for interim use in fast breeder reactor programs in the U. S. Since it does not constitute a final report, it should be cited as a reference only in special circumstances, such as requirements for regulatory needs.~~

Reactor Analysis and Safety Division
ARGONNE NATIONAL LABORATORY
9700 South Cass Avenue
Argonne, Illinois 60439

TABLE OF CONTENTS

	Page
LIST OF FIGURES	v
LIST OF TABLES	vi
ABSTRACT	vii
I. INTRODUCTION	1
II. FUNDAMENTAL PHENOMENA	2
A. Temperature Effects	2
B. Core Restraint System Design	4
C. Single Subassembly Example	9
D. Irradiation Effects	13
III. METHODS FOR CALCULATING RADIAL CORE DISPLACEMENT AND REACTIVITY FEEDBACK	15
A. The NUBOW-3D Computer Code	15
B. A Simple Expression for Reactivity Feedback	16
IV. SINGLE ASSEMBLY MODELLING IN SASSYS AND SAS4A	18
A. Model Overview	18
B. Subassembly Modelling and Equations	21
1. Reference Geometry and Temperatures	21
2. Governing Equations for the Subassembly Displacement	25
3. Subassembly Shape Calculation	27
4. Steady-State and Transient Calculations	40
5. Reactivity Worth Curve	42
C. Additional Modelling Options	43
1. Residual Clearance in the Core Interior	43
2. Additional Clearance at the Top Load Pads	44
3. Optional Behavior of the Exterior Subassemblies	44

TABLE OF CONTENTS (Cont'd)

V. SASSYS MODELLING FOR FFTF..... 46

A. Modelling the FFTF Core Restraint..... 46

B. Steady-State Model Validation in FFTF..... 47

C. Transient Model Validation in FFTF..... 56

1. FFTF GEMs Tests..... 56

2. FFTF Flow Transient Experiment..... 56

D. Modelling of FFTF with the Proposed Metallic Fuel Design.... 58

VI. CONCLUSIONS..... 63

REFERENCES..... 64

LIST OF FIGURES

No.	Title	Page
1.	Typical Subassembly Design for a Limited-Free-Bow Core Restraint System	3
2.	Typical Subassembly Temperature Distributions and the Resulting Unrestrained Subassembly Deflection	5
3.	Limited Free-Bow Core Restraint System Design	7
4.	Core Restraint System Design for FFTF	8
5.	Single Subassembly Model Schematic	10
6.	Subassembly Shapes for Various Power-to-Flow Ratios	12
7.	Subassembly Shapes for Various Core Loading States With the Subassembly Free to Tilt at the Grid Plate	29
8.	Subassembly Shapes for Various Core Loading States With the Subassembly Fixed at the Grid Plate	36
9.	Reactivity as a Function of Normalized Power-to-Flow Ratio in FFTF	53
10.	Subassembly Shapes in FFTF for Several Ranges of Normalized Power-to-Flow Ratio	54
11.	Calculated and Observed Reactivity as a Function of Time for an Unprotected LOF with GEMs from 50% Power and Nominal Flow	57
12.	Calculated and Observed Reactivity as a Function of Time for the FFTF Flow Transient Experiment	59
13.	Reactivity as a Function of Normalized Power-to-Flow Ratio in FFTF for the Proposed Metallic Fuel Core with 316 SS and HT-9 Load Pads	61

LIST OF TABLES

No.	Title	Page
1.	Input Data for the Radial Core Expansion Reactivity Feedback Model	22
2.	Model Designation for Core Shapes Calculated During the Steady-State and the Transient	41
3.	Nominal FFTF Core Restraint System Dimensions for the Current Oxide Fuel Core	48
4.	SASSYS and SAS4A Input for the Core Restraint Model of FFTF	49
5.	Code Modifications for Modelling FFTF	50
6.	FFTF Core Subassembly and Restraint System Geometry Changes for the Metallic Core with HT-9 Load Pads	60

ABSTRACT

The radial core expansion reactivity feedback model in SASSYS and SAS4A is reviewed, including background information, the fundamental phenomena, and a detailed discussion of the model and its options. All of the possible core loading configurations treated in the model are covered. A brief explanation of the algorithm is also included. The application of the model to the FFTF reactor is discussed in detail. The validation of the model with FFTF experimental results is presented for both steady-state and transient conditions. The estimate of the radial core expansion reactivity feedback for the proposed metallic fuel core in FFTF is provided, along with the underlying assumptions and cautions.

I. INTRODUCTION

The present emphasis on inherent safety for liquid-metal cooled reactor designs has resulted in a need to represent the various reactivity feedback mechanisms as accurately as possible. The response of a given reactor to any change in conditions is controlled by the magnitude and timing of these feedback mechanisms. The dominant reactivity feedback, which is usually negative and thus especially important in unprotected transients, has been found to result from radial expansion of the reactor core. In the present context, radial expansion means any change in the radial dimensions of the reactor core. An increase in the radial dimensions of the core is associated with a reduction in the reactivity of the core, or a negative reactivity feedback.

Since this component of the total negative reactivity feedback is dominant, emphasis has been placed on improving the understanding of this phenomenon with the goal of being able to implement a more mechanistic model into the SASSYS [1] and SAS4A [2] computer codes. This report documents the present level of understanding that was used to develop the current SASSYS/SAS4A model [3], and reviews the modelling details on the Fast Flux Test Facility (FFTF) along with some of the validation exercises that have been conducted to date [4,5,6]. As an introduction to the general subject of radial core expansion, a few basic concepts are reviewed first mainly for the purpose of establishing a common terminology for the phenomena involved. This is not intended to be an exhaustive review, but only to provide an introduction for explaining the SASSYS/SAS4A model. After this brief discussion, a short background summary is provided on some of the previous models used to calculate the reactivity feedback from radial core expansion. The current SASSYS/SAS4A model for radial core expansion reactivity feedback is discussed in detail, including modelling options. The validation with FFTF data is also reviewed, and the best estimate for the metallic fuel core in FFTF is covered.

II. FUNDAMENTAL PHENOMENA

The driving force behind radial expansion of the reactor core is temperature, whether a change in a temperature, or a change in a temperature gradient. These temperature changes then cause a change in the dimensions associated with the structures in the core. As will be shown in the following, it is these variations in dimensions and the resulting changes in the interactions between the subassemblies and the structures surrounding the core that control the radial size of the core. While this process can be quite complicated if all of the details for an entire core are considered, especially if generally minor effects such as load pad friction and load pad deformations are included, a simple example can be used to demonstrate the thermal effects. A particular subassembly geometry will be considered for most of the discussion, but the general behavior would apply to any design.

A. Temperature Effects

As an example to demonstrate the temperature effects, consider a single subassembly of the core, as shown schematically in Fig. 1. The subassembly consists of a hexcan duct containing the fuel pins. The hexcan duct has a fixture at the lower end to facilitate a connection to the core support plate, or grid plate. For this simple example, it will be assumed that the subassembly is held in a certain radial position at the grid plate, but that it is free to pivot, or tilt. There are two load pads, one at the top and one just above the top of the core, typical for a limited free-bow design. The subassembly load pads are regions along the duct wall which are thickened to provide a minimum spacing of the subassemblies and to withstand the loads generated by the interaction of the subassemblies with each other and with the structures around the core.

Assuming that the assembly is new, it will be nominally straight when inserted into the reactor. Since the primary system in the reactor is essentially isothermal at refueling temperatures and at hot standby temperatures, there are no thermal gradients in the system and the subassemblies will remain straight. However, since the refueling and hot standby temperatures are greater than nominal room temperature, the overall dimensions of the subassembly will increase slightly according to the thermal expansion coefficient for the material.

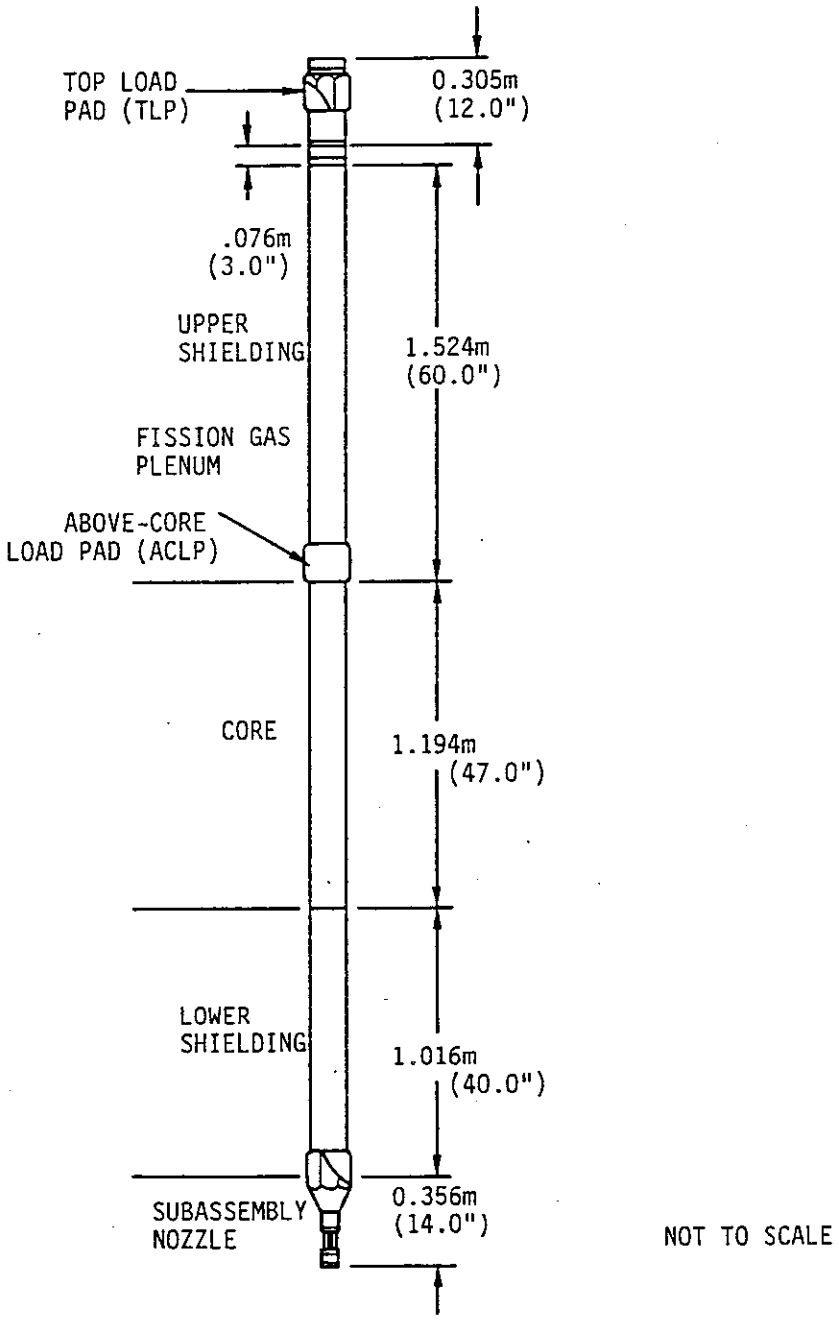

Fig. 1. Typical Subassembly Design for a Limited-Free-Bow Core Restraint System

As power is increased, the subassembly will experience an axial temperature gradient through the core region. An idealized axial profile of the coolant temperature is shown on Fig. 2, where the coolant temperature increases linearly through the core region and then remains constant to the top of the subassembly. There is some uncertainty about the behavior of the average coolant temperature in the upper regions of the subassembly, but the uncertainty in that region is not particularly important as the results are not very sensitive to it. For simplicity, constant temperature is a reasonable assumption. This axial temperature rise increases the temperature and the size of the above-core and top load pads on the subassembly. However, in a reactor, there are also temperature gradients in the horizontal direction, both radially and circumferentially. These temperature gradients arise from the radial and azimuthal variations in power generation, both between subassemblies and within any given subassembly. These temperature gradients will cause a deflection of the subassembly from the vertical, in that one wall of the hexcan will have a higher temperature and subsequently longer length than the opposite wall. The temperature gradient is zero in the lower regions of the subassembly, increases linearly through the core region, and is assumed to be constant in the upper regions. Again, the result is not particularly sensitive to this assumption. At any point, changes in power will cause the radial temperature gradients to change in proportion to the power, as the axial temperature profile does. The direction this deflection will take depends on the direction of the temperature gradient. As a simple example, for the direction shown in Fig. 2, the subassembly will deflect as indicated.

This behavior is typical for each subassembly in the reactor, yet there are differences in the axial temperature rise, and in the magnitude and direction of the radial temperature gradient for each subassembly. The particular shape of the subassembly is also modified in the reactor by the presence of other subassemblies and structures which surround the core. Before considering these effects in detail, a brief description of the core restraint system is given.

B. Core Restraint System Design

The core restraint system is designed to provide a confined geometric boundary for the core assemblies which facilitates loading and refueling, and

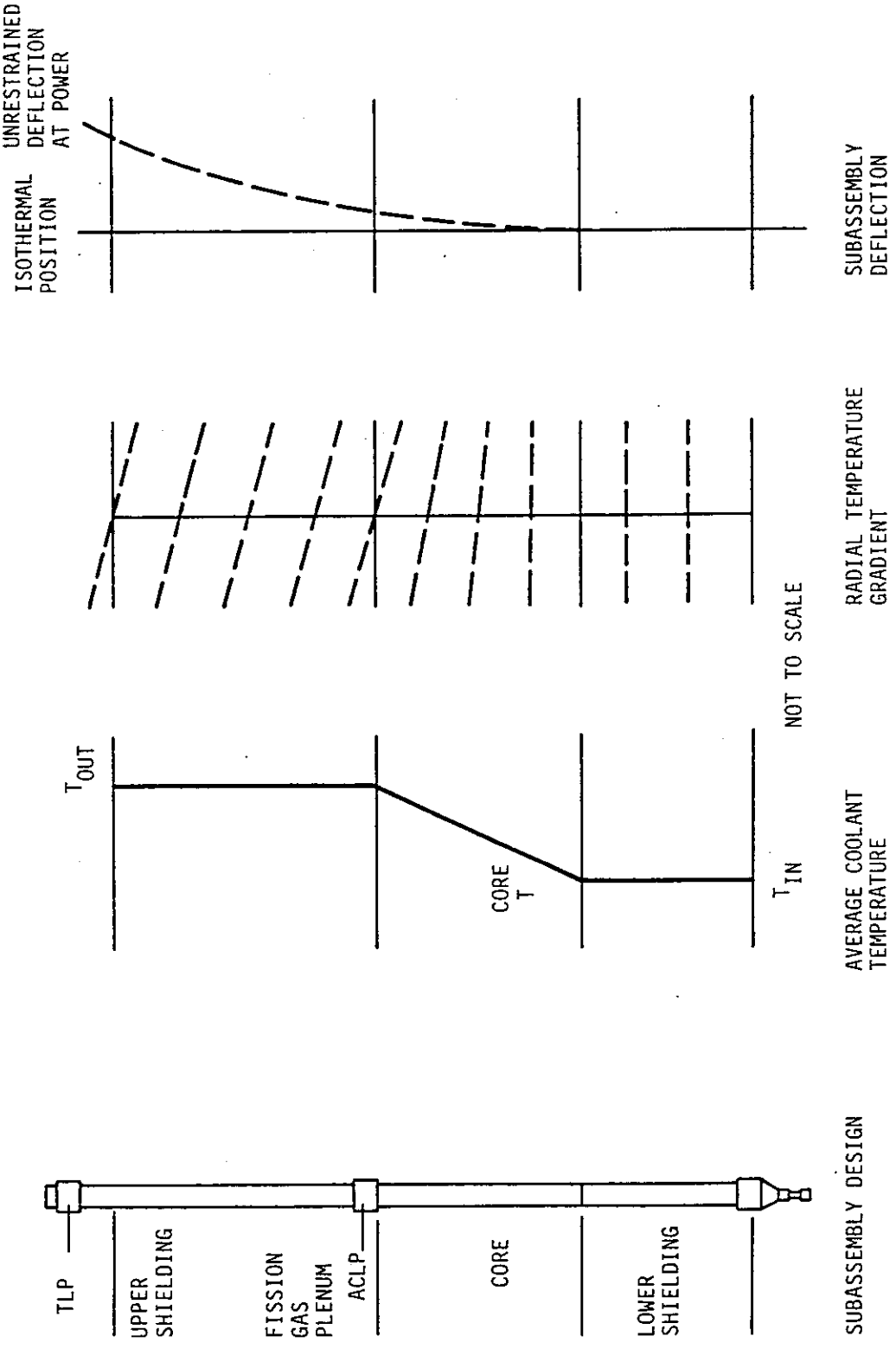

Fig. 2. Typical Subassembly Temperature Distributions and the Resulting Unrestrained Subassembly Deflection

it provides an upper limit on the size of the reactor core. It also interacts with the core assemblies to define the core geometry during operation, and is essential for assuring reactivity feedback from radial core expansion. The restraint considered in this report can be visualized as a ring, or rings, which surround the core at one or more elevations. The ring(s) may be segmented around the core and attached to the core barrel.

The driver, blanket, reflector, shield, and control assemblies have load pads at the elevations of the restraint rings and at other elevations as required. In general, the number and location of the subassembly load pads varies from one design to the next, as do the number of core restraints. While there is no unique arrangement for the load pads and the core restraint, there are some arrangements which result in a much more favorable reactivity feedback from radial core expansion. The schematic shown in Fig. 3 is typical of a limited free-bow core restraint design, and is currently a preferred arrangement. The core restraint ring is attached to the core barrel, providing a solid boundary for the subassemblies. The subassembly used in Figs. 1 and 2 would be suitable for this type of core restraint. This design is currently proposed for advanced liquid metal reactors (LMRs). A similar design is used in FFTF, although the FFTF has two core restraint rings, as shown in Fig. 4. The presence of the additional restraint ring limits the maximum size of the above-core load pad region, limiting the magnitude of the reactivity insertion resulting from a sudden core compaction. It is also designed to improve the seismic response by preventing large changes in the core dimensions. The FFTF design has the upper restraint ring attached to the core barrel, while the lower ring is essentially free to move in the radial direction and is not solidly attached to the core barrel, but is supported by the inner shielding.

The core restraint system is designed to facilitate insertion and removal of assemblies by having a net clearance between the size of all of the core assembly load pads and the restraint ring. This is shown schematically in Figs. 3 and 4, where all of the subassembly load pads have been pushed together so that all of the clearance occurs between the last assembly and the restraint ring. With isothermal conditions in the reactor at refueling temperature, there are no temperature gradients to bend the subassemblies and the clearances prevent excessive subassembly withdrawal forces, although this is

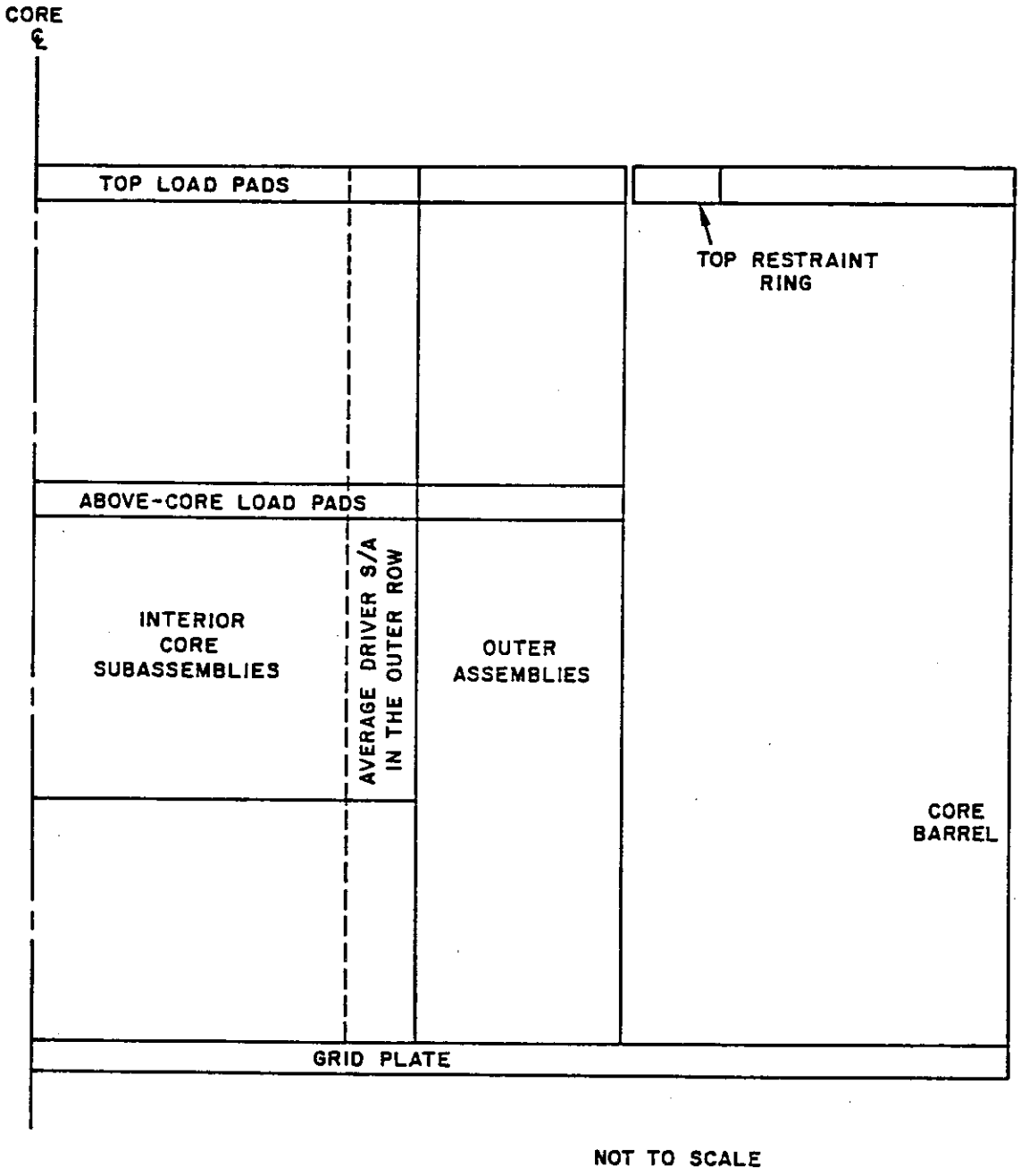

Fig. 3. Limited Free-Bow Core Restraint System Design

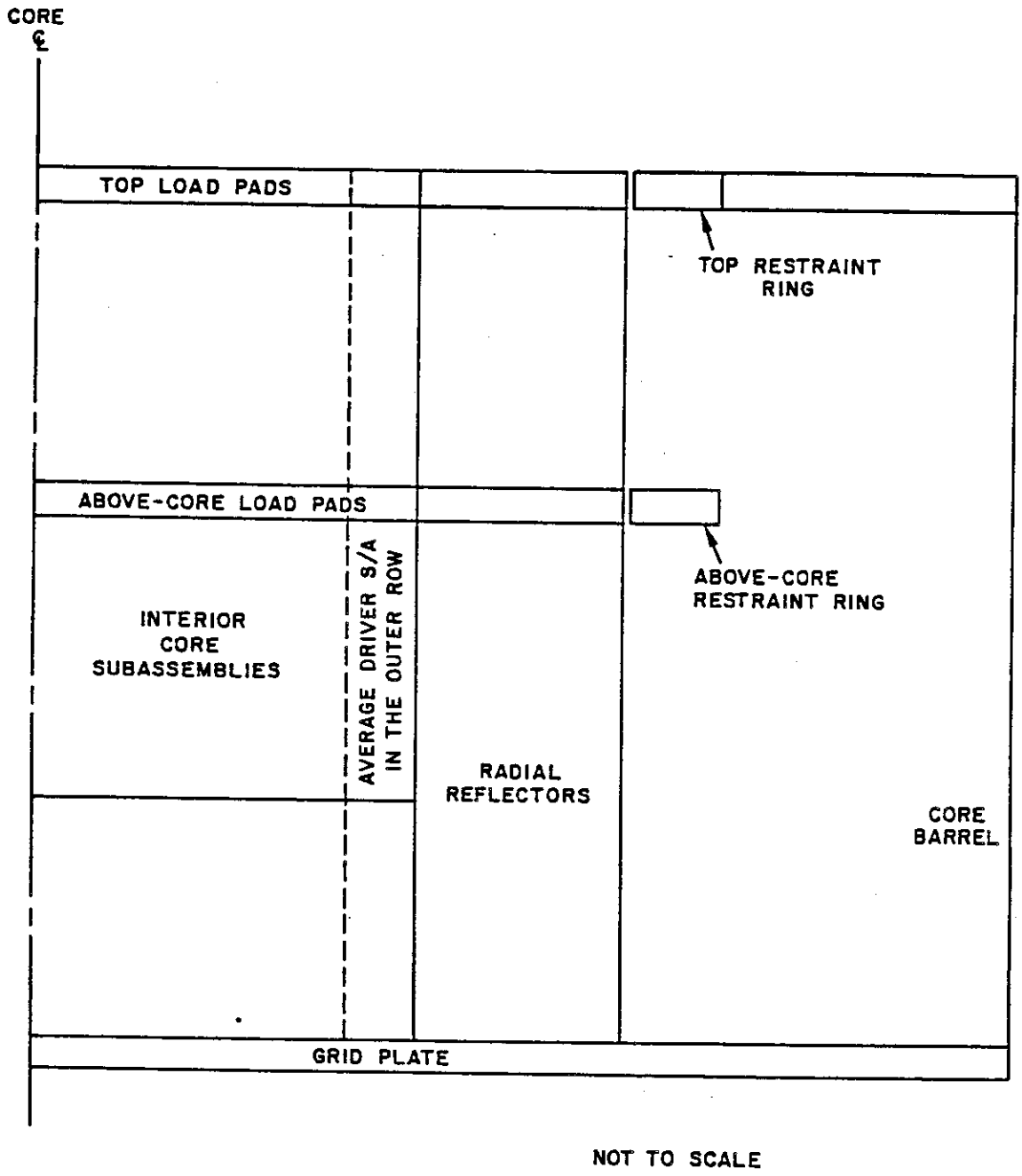

Fig. 4. Core Restraint System Design for FFTF

complicated by irradiation effects. The increase in temperature up to hot standby conditions also preserves these clearances since this is also an isothermal condition. However, the clearances may be modified under these conditions by the use of different materials for the various structures, such as 316 SS for the core restraint ring and HT-9 for the subassemblies. The lower thermal expansion coefficient for HT-9 will cause the clearances to increase for an isothermal temperature increase.

The presence of clearances at hot standby conditions implies that the position of the subassemblies within the restraint ring is not defined, i.e., there is a range of possible radial locations for the top of the subassemblies within the boundary provided by the restraint ring. In general, there would be a random distribution of the clearance among all of the subassemblies. As a result of this clearance, the radial position of the subassemblies containing the active fuel is not defined either. The reactivity variation associated with this uncertainty in position is not necessarily small depending on the clearances at the restraint ring. In the absence of irradiation effects which permanently deform the subassemblies, the only way to close up the clearances and have the position of the assemblies well- defined is to have bending of the subassemblies caused by the temperature difference of opposite sides of the subassembly hexcan, as described in Section II-A.

This background information is sufficient for examining the behavior of any particular subassembly in the reactor. Before considering the effects of irradiation creep and swelling, a simple example will be used to demonstrate the interactions of the temperatures, temperature gradients, and core restraint.

C. Single Subassembly Example

The behavior of a single subassembly can be investigated with a model as shown on Fig. 5. The single subassembly represents one from the row with the largest average radial temperature gradient. There are subassemblies in the interior of the core with relatively little temperature gradient, and subassemblies in the exterior regions which also have small radial temperature gradients. As described above, there will be randomly distributed clearances in the core with the result that the position of any particular subassembly is not defined, but rather it can occupy a certain range of radial positions.

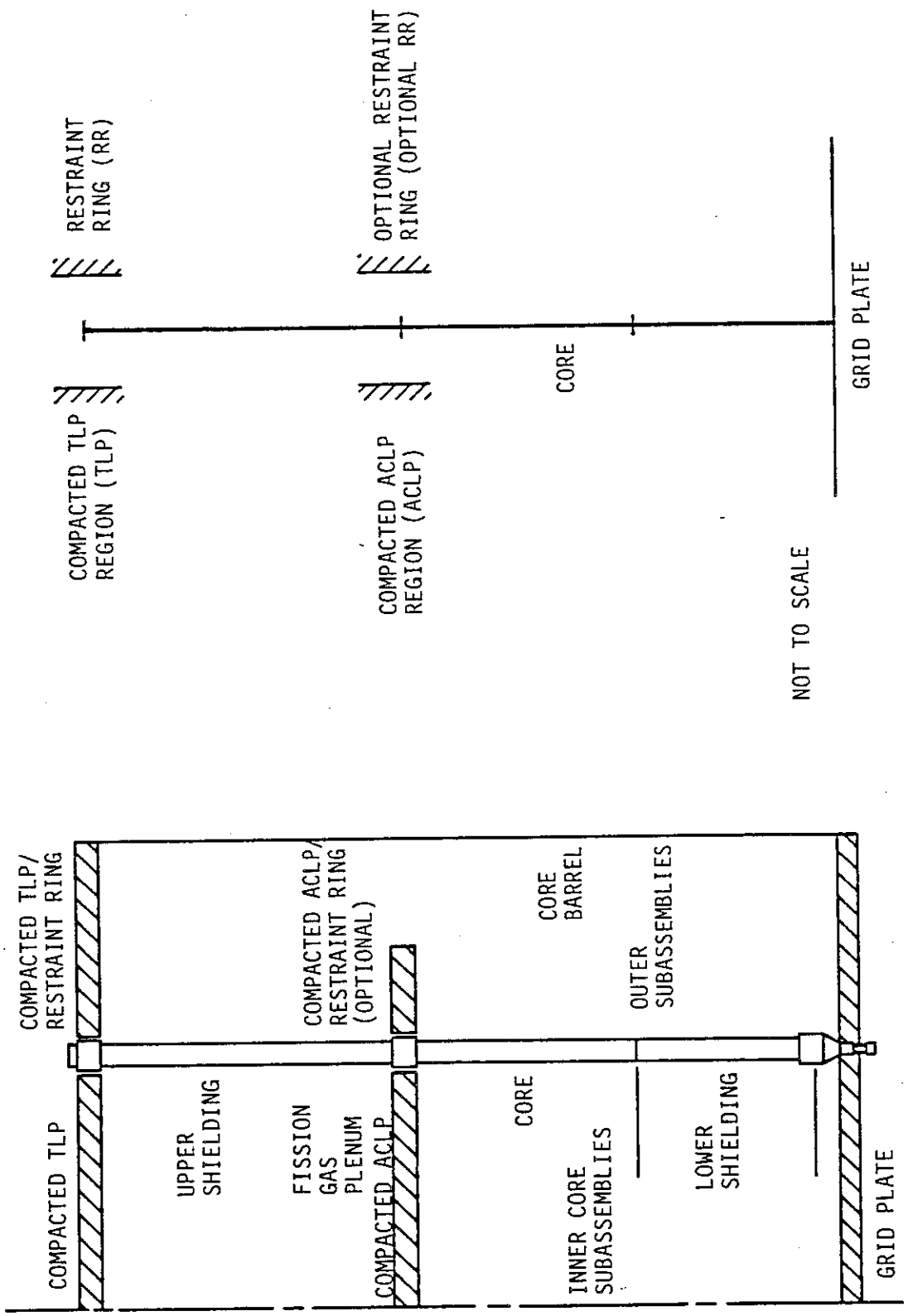

Fig. 5. Single Subassembly Model Schematic

The largest possible range of positions for the single subassembly is obtained by pushing together, or compacting, all of the subassembly load pads for those subassemblies interior to the single subassembly being considered, and pushing all of the assemblies exterior to it out against the restraint ring. For this simple example, it is assumed that the load pads will all go together perfectly, i.e., ideal packing. This provides the maximum clearance for the single subassembly shown in Fig. 5. Constant flow rate through the core will also be assumed for this example, and the subassembly is assumed to be vertical at the grid plate until there is a mechanism to cause it to tilt.

A schematic representation for this model is also shown on Fig. 5. This schematic will be used in the remainder of the report. It is assumed that the compacted load pad regions in the interior of the core provide solid boundaries. The combination of compacted top load pads in the exterior of the core and the restraint ring is assumed to provide another solid boundary, as shown. The same is true for the above-core restraint ring, if present. The position of the boundaries is a function of the temperature of all of the components involved, and so may not remain fixed in space as a function of time during a transient, depending on the time constants. The boundaries are assumed to remain solid, however. The clearances are greatly exaggerated in order to show the displacements and load pad contacts clearly.

As power is increased, the temperature rise through the core is established, along with the radial temperature gradient. This causes the subassembly to deflect at the ACLP and the TLP. It also increases the size of the compacted load pad regions. The deflection of the subassembly and the growth of the load pads reduce the available clearance and the possible range of subassembly positions becomes smaller, as shown in Fig. 6a. All of the other assemblies deflect as well, and as long as the temperature gradients are generally in the same direction they have no effect on the clearances. As power is increased further, the bending of the subassembly and increased size of the load pads are sufficient to close the gaps at the ACLP and TLP, as shown in Fig. 6b. Once the gaps have been closed, the position of the subassembly is well-defined. This also implies that the position of all of the other subassemblies is determined as well. Note that the core region has moved inward as the gaps closed, which would cause the core reactivity to increase. For higher powers, the core will have a well-defined size, which has a number of consequences both for control and for safety considerations.

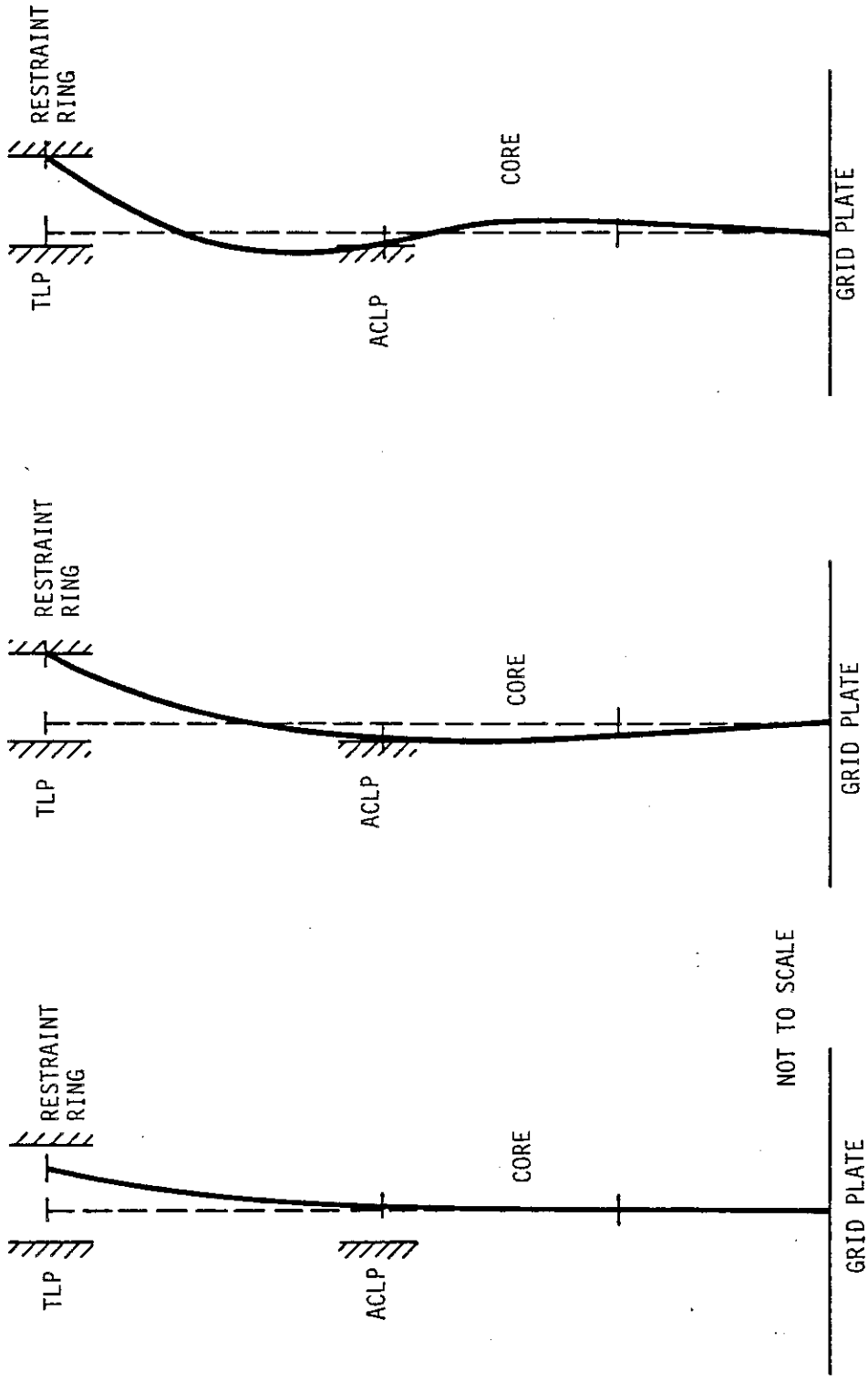

A. LOW POWER-TO-FLOW RATIO B. MODERATE POWER-TO-FLOW RATIO C. NOMINAL POWER-TO-FLOW RATIO

Fig. 6. Subassembly Shapes for Various Power-to-Flow Ratios

It is considered desirable to have the power at which the core geometry is well-defined be less than nominal power and flow conditions, so that one is assured of having a defined geometry at nominal power throughout the life of the core, yet not too low which would create large intersubassembly forces at nominal power.

As power is increased beyond the point where all of the available clearances have been taken up, the subassembly begins to take a different shape. Since the bending due to the radial temperature gradient continues to increase and the load pads continue to expand with increases in power, yet there is no room to accommodate the larger deflections, forces are generated at the load pad regions and the subassembly is elastically bent as a result. There is a compressive force at the ACLP into the interior of the core region, and a compressive force at the TLP out to the restraint ring. Generally, the higher the power, the larger the forces. The shape is shown on Fig. 6c for an arbitrary power, which could be considered as nominal power. The shape is determined by treating the subassembly hexcan as an elastic beam subject to the forces at the load pads and with the applied radial temperature gradient. Given the construction of the subassembly, the hexcan should behave as an elastic beam of basically uniform axial characteristics.

This behavior is typical of each assembly in the reactor. The particular shape that any subassembly will take depends on the magnitude and direction of its radial temperature gradient, and the corresponding behavior of the surrounding subassemblies. However, by focusing on the subassemblies with the largest gradients, and if the other assemblies deflect in the same direction, in general, it is possible to ignore these interactions for the purpose of determining the core size.

D. Irradiation Effects

The irradiation of the subassembly hexcan during operation can have a significant impact on the interactions between subassemblies and the core restraint system. Regardless of whether creep or swelling is involved, the result is to bend the subassembly in an inelastic manner. With reference to Fig. 5, if the subassembly is not straight initially, this has the effect of changing the available space that the subassembly may take. This change can also be modified by similar irradiation effects on the neighboring subassemblies.

The inelastic deformation occurs in the core region of the subassembly, with the remaining portions of the subassembly remaining straight. Depending on the flux gradient, the temperature gradient, and the creep or swelling of the hexcan, the deformation can be either inward or outward with respect to the core centerline. For the case where the subassembly is bent outward by the effect of irradiation, and the radial temperature gradient is in the same direction as in Figs. 2, 5 and 6, the power at which the bending of the subassembly is sufficient to close the available gap is lower than for the unirradiated assembly. This can be thought of as having the irradiated shape of the subassembly being roughly equivalent to a shape at some power. The difference between this power and that required to close the gaps is less than the difference when starting with a straight assembly at zero power. For the case where the subassembly is bent inward, the power required is higher, perhaps even greater than nominal power depending on the design. This is because some power level is required to bring the subassembly back to being approximately straight. In general, current designs with the clearances being initially closed at a normalized power-to-flow ratio of 0.7 can easily shift this value from 0.6 to 0.8 or more during the life of the core because of these effects [7-10].

With this review of the basic phenomena, the previously available methods for calculating core displacements and the associated reactivity feedback are discussed in the next section. The focus of this discussion is to provide the additional perspective from which the current SASSYS/SAS4A model was developed, as described in Section IV.

III. METHODS FOR CALCULATING RADIAL CORE DISPLACEMENT AND REACTIVITY FEEDBACK

Several methods were being used to calculate the reactivity feedback from radial core expansion, ranging from very simple concepts to detailed computer codes. As examples of the available models, two models are described in this section, a simple model and the computer code NUBOW-3D. These models not only cover the range of possible models, they are at the two extremes in complexity. Unfortunately, very little was available between these two models in terms of complexity.

A. The NUBOW-3D Computer Code

At the time when the current detailed model for SASSYS and SAS4A was being developed, most of the calculations for determining reactivity feedback from radial core expansion were being done with NUBOW-3D [7-10, 11, 12]. The NUBOW-3D computer code models every subassembly within a certain sector of the reactor, and attempts to include all of the behavior for individual assemblies and their interactions, along with creep and swelling effects. The code was originally designed for studying core design and reloading, where these details are essential for ensuring that the reactor core can be loaded and reloaded without generating excessive subassembly insertion and withdrawal loads. It was also realized that since NUBOW-3D contained all of the structural behavior of the subassemblies, it should be possible to calculate the associated reactivity changes using the displacement worth for each subassembly. While the means for obtaining accurate displacement worths for this method is still being studied, results were obtained with the best estimates available and provided clues to the important structural phenomena [7-10]. Of particular interest was the importance of the core loading state on the core displacement, that is, when the clearances have been taken up, as shown in Fig. 6, the change in the effective core radius for a given change in power is markedly increased due to the additional bending of the subassembly. This has a pronounced effect on the course of certain unprotected transients, since greater negative reactivity feedback is available for limiting the effects of the transient. Insight from the numerous NUBOW-3D calculations was also used to define the discussion of the important fundamental phenomena given in Section II. Some of the other effects considered by NUBOW-3D but not reviewed are load pad compressibility and load pad friction, which were not believed to be important for the current designs being studied.

The NUBOW-3D code is a powerful tool for analyzing the structural interactions in the core, and can be used for reactivity changes when accurate displacement worths are available. However, the details which make NUBOW-3D so useful for such work also make it difficult to adapt for calculations of operational transients or accident situations since the code calculations require significant amounts of computer time for each condition. A slightly simpler variant of NUBOW-3D, called NUBOW-2D, was developed which models the reactor core as a series of rows, rather than individual subassemblies, but is not significantly simpler or faster numerically than NUBOW-3D. As a result, neither approach was considered for connecting into SASSYS and SAS4A. The detailed modelling in NUBOW-3D would also be inconsistent with the level of detail incorporated in the current SASSYS and SAS4A codes for modelling the core. For these reasons, a simpler, much faster, method was sought which would provide essentially the same result as an accurate NUBOW-3D calculation but was more suited for incorporation into SASSYS and SAS4A.

B. A Simple Expression for Reactivity Feedback

Perhaps the simplest expression for determining the reactivity feedback from radial core expansion is the one recommended by Madell [13]. The equation is given as follows:

$$\Delta\rho_{rc} = C_{rc}\left[\Delta T_{in} + \frac{XMC}{XAC}\left(\Delta T_{out} - \Delta T_{in}\right)\right]$$

where

$\Delta\rho_{rc}$ = reactivity change due to the effective change in core radius, \$

C_{rc} = reactivity feedback coefficient, \$/K

ΔT_{in} = change in the core inlet temperature, K

ΔT_{out} = change in the core outlet temperature, K

XMC = distance from the nozzle support at the bottom of the subassembly to the core midplane, m

XAC = distance from the nozzle support at the bottom of the subassembly to the above-core load pads, m

This equation is included in SASSYS [1] and SAS4A [2] and is identified as the simple radial core expansion reactivity feedback model. The calculation of reactivity feedback is based on the displacement of the core midplane, where the reactivity feedback coefficient is based on the thermal expansion of the load pads. The factor XMC/XAC is the geometric relationship between the load pads and the core midplane with respect to the grid plate. The main drawback of this method is that it does not calculate an actual core displacement and as a result is unable to account for changes in core loading states. It also only includes the reactivity feedback from load pad thermal expansion since the feedback coefficient is based on a uniform dilation of the core, yet NUBOW-3D results usually indicate 30-40% more feedback due to additional subassembly bending caused by interaction with the core restraint as shown in Fig. 6. This can be artificially included upon comparison with NUBOW-3D results by changing the reactivity feedback coefficient but the range of applicability would be unknown during a transient.

This simple formulation for the reactivity feedback contains one of the basic assumptions employed in the current SASSYS/SAS4A detailed model, namely that the reactivity feedback from radial core expansion can be represented as being proportional to the change in the overall size of the core without considering the details of the motion of individual assemblies as in NUBOW-3D. For the SASSYS/SAS4A detailed model, this is incorporated by having the reactivity change proportional to the change in the equivalent radius of the core, but where the core radius is a function of axial position. This assumption makes it possible to perform a considerable simplification over the much more involved calculations represented, for example, by NUBOW-3D, yet still retain some of the basic structural modelling so that changes in core loading state or in bending caused by subassembly/core restraint interaction can be calculated.

IV. SINGLE ASSEMBLY MODELLING IN SASSYS AND SAS4A

The radial core expansion reactivity feedback model in SASSYS and SAS4A is based on the simplicity obtained with the simple radial core expansion model, yet incorporating as many of the important details from NUBOW-3D as possible. The result at present is a single assembly model, referred to as the detailed radial core expansion model in SASSYS and SAS4A. Basically, a single subassembly is selected from a row with a high worth for radial motion, and is treated as a simple beam as described in Section II. This subassembly is then subjected to an appropriate radial temperature gradient, along with clearances to the various parts of the core restraint system, to determine its shape at steady-state and at any time during the transient. The change in shape is then related to the reactivity feedback. This model is intended to be a combination of the best features of the simple and complicated models, creating a model that is detailed enough for transient and accident calculations, yet simple enough to run rapidly as part of an accident analysis code.

A. Model Overview

The key to the detailed radial core expansion model in SASSYS and SAS4A is the ability to select a subassembly which contains not only the high radial displacement worth but also substantial temperature gradients in the radial direction. In general the combination of these two features would be expected. In a reactor core, the neutron flux and thus the power generation is relatively flat over a wide area in the interior of the core. There may be localized variations, such as around control subassemblies, but on the average these are not widespread. As a result, the reactivity change associated with any motion of the subassemblies in the interior of the core is not particularly large. In the case of the localized concentrations of subassemblies, there are usually as many subassemblies moving in one direction as there are moving in the opposite direction, with canceling reactivity effects. Near the edge of the active region of the reactor core, there is a large change in the flux across the assembly, leading to a large gradient in the power production in such assemblies. The displacement worth of these assemblies is large, contributing perhaps 90% of the total reactivity change for a uniform expansion of the core, i.e., where all of the assemblies are moved outward propor-

tional to their distance from the center of the core. The subassemblies which contain these large gradients are usually either the outermost row of driver subassemblies, or the next row out, such as radial blankets.

The radial temperature gradient across an assembly is also strongly affected by the gradient in power. The temperature of any particular wall of the hexcan is determined by heat transfer with adjacent subassemblies and by the heat produced in the row of fuel pins next to that wall. The dominant effect appears to be the heat generation in the fuel pins, with the heat transfer occurring as a secondary effect. In this way, a subassembly with a large gradient in power will also have a large difference in the temperature of opposite walls. As a result, the outermost row of drivers not only has a large displacement worth as a result of the large flux gradient, but it also has a large temperature gradient for the same reason. Given this situation, it is possible to use such an assembly as an indicator of the change in the reactivity of the core due to changes in size.

The basic strategy followed with this model can be summarized by the following series of steps:

1. A subassembly in the outermost row of drivers is selected for the calculation, although it possibly could be in the first row of radial blankets, if desired.

2. The radial temperature gradient across this assembly is taken as the average of the gradients for all assemblies in the outer row of drivers. This should provide an average displacement of the assemblies in the outer row.

3. Given the dimensions, materials, and temperatures for all of the subassemblies and structures in the core, the net clearance available for displacement is determined, as in Fig. 5.

4. Based on the results of steps 2 and 3, the possible core configurations can be established, in a manner similar to that used for Figs. 5 and 6.

5. With such a calculation determining the axial profile of the active core boundary at steady-state, identical calculations for every step of the transient provide a detailed history of the change in the size of the core.

6. Using the change in dimensions of the core along with the axial distribution of the radial expansion worth for the core, the reactivity change is calculated at every step of the transient.

The underlying assumptions for this process are as follows:

1. The reactivity of the core is predominantly determined by the total volume of the core. Details of the subassembly displacements in the interior of the core have only a small effect on the reactivity.

2. The variation in radial temperature gradient from one subassembly to the next around the periphery of the core (the outermost row of drivers) can be represented by an average radial temperature gradient applied to the single subassembly in the model.

3. The variation in the shape of the core around the periphery can be represented by an average axial profile generated by the single subassembly in the model. The reactivity change during a transient is not dependent on the details of the core shape around the periphery of the core.

4. The displacements of the other subassemblies in the core are proportional to their distances from the center of the core. This is only important for the step where the reactivity feedback is calculated, where the fuel at each elevation is distributed uniformly in the radial direction.

With this approach, it is possible to do a rapid, detailed calculation of the average core shape at every step of a transient, and also accommodate any changes in core loading that may occur.

B. Subassembly Modelling and Equations

The single subassembly represented in the SASSYS/SAS4A detailed radial core expansion model is shown in Fig. 5. The subassembly is the same as that shown in Fig. 1, since the present version of the model is applicable to limited free-bow designs such as the advanced LMRs, and FFTF. A general version of the model is being developed based on the same principles for use with other reactor designs. As in Fig. 1, the subassembly has two load pads, an ACLP just above the core and a TLP just below the top of the subassembly. The subassembly hexcan is treated as an elastic beam with uniform properties in the axial direction. The corresponding differential equation for calculating the shape of the hexcan is then subject to a variety of boundary conditions. For any particular set of boundary conditions, the equation is solved to yield an algebraic expression for the shape of the beam. The shape through the core region used for the reactivity feedback is not the axis of the outermost driver, however, but the outer edge of this assembly out to the load pad dimension. This curve then contains all of the active fuel region within it.

Using this model, the major task is to develop the algorithm for selecting the proper set of boundary conditions during the steady-state and the transient. The following sections describe the algorithm along with the algebraic expressions used for each case. For completeness, all possible core loading configurations have been included even if the current understanding of core loading behavior and the expected temperature fields may not create conditions which lead to some of these configurations.

1. Reference Geometry and Temperatures

There are several calculations needed to initialize the model. The set calculates all of the required core geometry, at a reference temperature which is specified by input and is usually 300 K. The data required for this step are listed in Table 1. For further details, refer to reference 1. Information on basic dimensions and materials are needed at this stage. The expressions for thermal expansion are included in the code for 316 SS (which also serves as an approximation for D-9) and HT-9. Given the basic input data, the following reference dimensions are calculated:

Table 1. Input Data for the Radial Core Expansion Reactivity Feedback Model

Variable	Description
IRADEX	Integer to select appropriate radial core expansion reactivity feedback model
NSUBTC	Total number of subassemblies in the active core region, including control and internal blanket assemblies
NSUBTR	Total number of subassemblies in the reactor, including drivers, radial and internal blankets, control assemblies, radial reflectors and shields
NRRNGS	Number of restraint rings in the core restraint system
NTGRD	Core support grid material
MTACLP	Above-core load pad material
MTTLP	Top load pad material
MTRRAC	Above-core restraint ring material
MTRRT	Top restraint ring material
MTRFAC	Outer assemblies above-core load pad material
MTRFT	Outer assemblies top load pad material
IROPT	Option for outer assemblies to push single assemblies inward
PITCHG	Subassembly pitch at the grid plate
PITCHA	Above-core load pad flat-to-flat dimension
PITCHT	Top load pad flat-to-flat dimension
ACLPRC	Clearance at the above-core load pad plane
TLPRRC	Clearance at the top load pad plane
BNDMM1	Thermal bending moment at the top of the core region
BNDMM2	Thermal bending moment in the above-core region
DFLTCS	Deflection of the top of the core region due to irradiation
DFLTSS	Deflection of the top of the subassembly due to irradiation
SLLMAX	Maximum allowable slope of the subassembly at the grid plate

Table 1 (Contd.)

RDEXCF	Radial core expansion uniform dilation worth
FCDTR1	Fraction of nominal core temperature rise applied to the above-core restraint ring
FCDTR2	Fraction of nominal core temperature rise applied to the top restraint ring
FCDTRF	Fraction of nominal core temperature rise applied to the load pads of the outer assemblies
RR1TC	Thermal time constant of the above-core restraint ring
RR2TC	Thermal time constant of the top restraint ring
CRSAC	Additional clearance in the core interior due to non-ideal packing of the subassemblies
DRCOLL	Additional clearance between the subassembly and its top load pad

1. grid plate equivalent radius
2. minimum above-core load pad equivalent radius
3. minimum top load pad equivalent radius
4. minimum outer assemblies equivalent radius
5. restraint ring(s) equivalent radius

The outer assemblies include all assemblies outside of the last row of driver subassemblies. The equivalent radius is obtained by calculating the cross-sectional area occupied by the structure, such as the load pads, and converting it into the equivalent circle maintaining the cross-sectional area. Since the input data are provided at a reference temperature, all of these dimensions are at the reference temperature as well.

The initial structure temperatures are calculated based on the steady-state core inlet temperature, the temperature rise through the core, and some input data. These are also listed in Table 1. The grid plate temperature is taken to be the same as the temperature of the walls of the inlet plenum when PRIMAR-4 is used, and the same as the coolant inlet temperature when PRIMAR-1 is used. At steady-state, these are essentially the same. The temperature of the restraint ring(s) is based on the coolant temperature rise through the core and input data. The same is true for the outer assemblies, identified as the 'reflector' region in the model.

The calculation for the load pad temperatures in the interior of the core is more involved. Due to the construction of the subassemblies, with fuel pins wrapped with spacer wires, there is more flow along the hexcan walls next to the outer row of pins than there is in the interior of the fuel pin bundle. This has the effect of overcooling the edge pins and the hexcan walls as compared to the average coolant temperature. Based on experimental evidence and code calculations with both COBRA-WC [14] and SUPERENERGY-2, a typical value in these edge regions is a 25% reduction in the temperature rise at full flow. Therefore, during the initialization, 75% of the average coolant temperature rise through the core is applied to the hexcan load pads. Using these temperatures for the load pads, the initial equivalent radius of the load pad regions is calculated using the thermal expansion coefficient from reference temperature up to the load pad temperature. These calculations define the dimensions of all of the important structures and

establish the maximum available clearance for the single subassembly at nominal power.

2. Governing Equations for the Subassembly Displacement

The subassembly displacement from the vertical can be given by the following equation:

$$EI \frac{d^2y}{dx^2} = M_x$$

where

E = modulus of elasticity, N/m^2
I = moment of inertia of the subassembly cross-sectional area, m^4
M_x = bending moment, N-m
x = distance along the subassembly, m
y = distance perpendicular to the subassembly, m

Since only the displacement is required from this equation, and the boundaries are solid, the solution is independent of EI. The forces and moments are dependent on the value of EI, however. The bending moment can be the result of forces at the grid plate or the load pads, or the flat-to-flat temperature difference of opposite sides of the subassembly hexcan.

The radial temperature gradient, or flat-to-flat temperature difference is input as an equivalent bending moment. This calculation in the core region and the above-core region is based on the average flat-to-flat temperature difference in the radial direction for the outermost row of driver subassemblies, each according to the following equation:

$$\frac{M_T}{EI} = \alpha \Delta T/D$$

where

M_T = thermal bending moment, N-m
α = subassembly hexcan thermal expansion coefficient, 1/K

ΔT = flat-to-flat temperature difference, K

D = subassembly hexcan flat-to-flat dimension, m

The bending moment is then used to calculate the deflection of the subassembly in the absence of any core restraint or interassembly effects. The irradiation effects are included in a similar manner, with an initial subassembly deflection at the top of the core and at the top of the subassembly being input. The code converts this into an equivalent bending moment, and is summed with the thermally-induced bending moment to yield a total bending moment in each region of the assembly:

$$M_1 = M_{1T} + M_{1I}$$

$$M_2 = M_{2T} + M_{2I}$$

where

M_{1I} = equivalent bending moment for irradiation effects in the core region, N-m

M_{2I} = equivalent bending moment for irradiation effects in the above-core region, N-m

M_{1T} = thermal bending moment in the core region, N-m

M_{2T} = thermal bending moment in the region above the core, N-m

The thermal bending moment is input as a bending moment since the flat-to-flat temperature difference would appear to be the known quantity. For irradiation effects, the subassembly deflections would most likely be known, and are used as the input. The relationship between the deflection at the top of the core and at the top of subassembly which ensures that all of the irradiation effects are confined to the core region is as follows:

$$y_{2I} = y_{1I} [1 + 3 (L-a)/(a-x_1)]$$

where

y_{2I} = displacement at the top of the subassembly, m
y_{1I} = displacement at the above-core load pad, m
L = length of the subassembly, m
a = elevation of the above-core load pad, m
x_1 = elevation of the core/lower reflector interface, m

This keeps the regions of the subassembly below the core and above the core straight in the absence of any forces from the load pads or restraint ring.

3. Subassembly Shape Calculation

The reference geometry, temperature field, and irradiation effects determine the shape of the subassembly. For the limited free-bow design, there are 15 possible core loading configurations, plus options, when there are two restraint rings as in FFTF. When only 1 restraint ring is present, there are 10 possibilities, plus options. A suitable algorithm is used to select the proper loading condition given the clearances and the temperature field. The subassembly deflection from the vertical at the ACLP and the TLP is determined from the bending moments, according to the following equations:

$$y_a = (M_1)\ (a-x_1)^2/6EI$$

$$y_L = \{(M_1)[(L-a)(a-x_1)/2 + (a-x_1)^2/6] + (M_2)(L-a)^2/2\}/EI$$

where

y_a = deflection at the ACLP, m
y_L = deflection at the TLP, m
M_1 = bending moment in the core region, N-m
M_2 = bending moment in the above-core region, N-m

At this point, the model contains logic to determine if the subassembly will fit in the available space or not. The same algorithm is used for either 1 or 2 restraint rings but some of the paths are not possible with only 1 restraint ring. The first step is to test if the deflection of the ACLP by thermal bending causes interference between the assembly and the compacted ACLP region in the interior of the core, or with the restraint ring at this elevation if

one is present, assuming that the subassembly is vertical at the grid plate. If there is no interference, a similar test is performed for the TLP. If there is interference, the subassembly is tilted to accommodate it and the clearance at the ACLP and TLP is tested again. Based on the result of these and further similar tests, the appropriate loading condition is established.

The process can be complicated by restricting the amount of tilting at the grid plate with the design of a tight coupling between the fixture at the bottom of the subassembly and the receptacle in the grid plate. The algorithm also tests for any limits imposed by such a design and modifies the subassembly loading accordingly. This forms the complete set of cases tested based on the initial thermal bending of the subassembly. In the following the details for each of the possible core loading states is reviewed, along with the equation and the implications on the reactivity feedback. The impact of the available options is also discussed.

Case 1: No Load Pad Contact at the ACLP, TLP, or Restraint Ring(s), Grid Plate/Subassembly Clearance Not Exceeded

For this case, the thermal bending of the subassembly is not sufficient to close the gaps at either the ACLP or TLP. This condition is illustrated in Fig. 7a, with the equation for determining the shape in the core region as follows:

$$y(x) = \frac{M_1}{6EI(a-x_1)} (x-x_1)^3 \qquad \text{for } x_1 \leq x \leq a$$

Since the clearances at the ACLP and TLP elevations are still present, the position of the subassembly is not uniquely determined, but can occupy a range of positions, similar to that discussed with Fig. 5. With no mechanism for establishing a position for the subassembly, the model assumes that the subassembly will be vertical at the grid plate. Within this restriction, an increase in power results in negative reactivity feedback from the larger core dimension due to the increase in the thermal bending. However, it should be emphasized that this assumption may not be valid, and such feedback would not be guaranteed. The magnitude of the feedback is small for this condition, as compared to the feedback obtained for thermal expansion of the load pads.

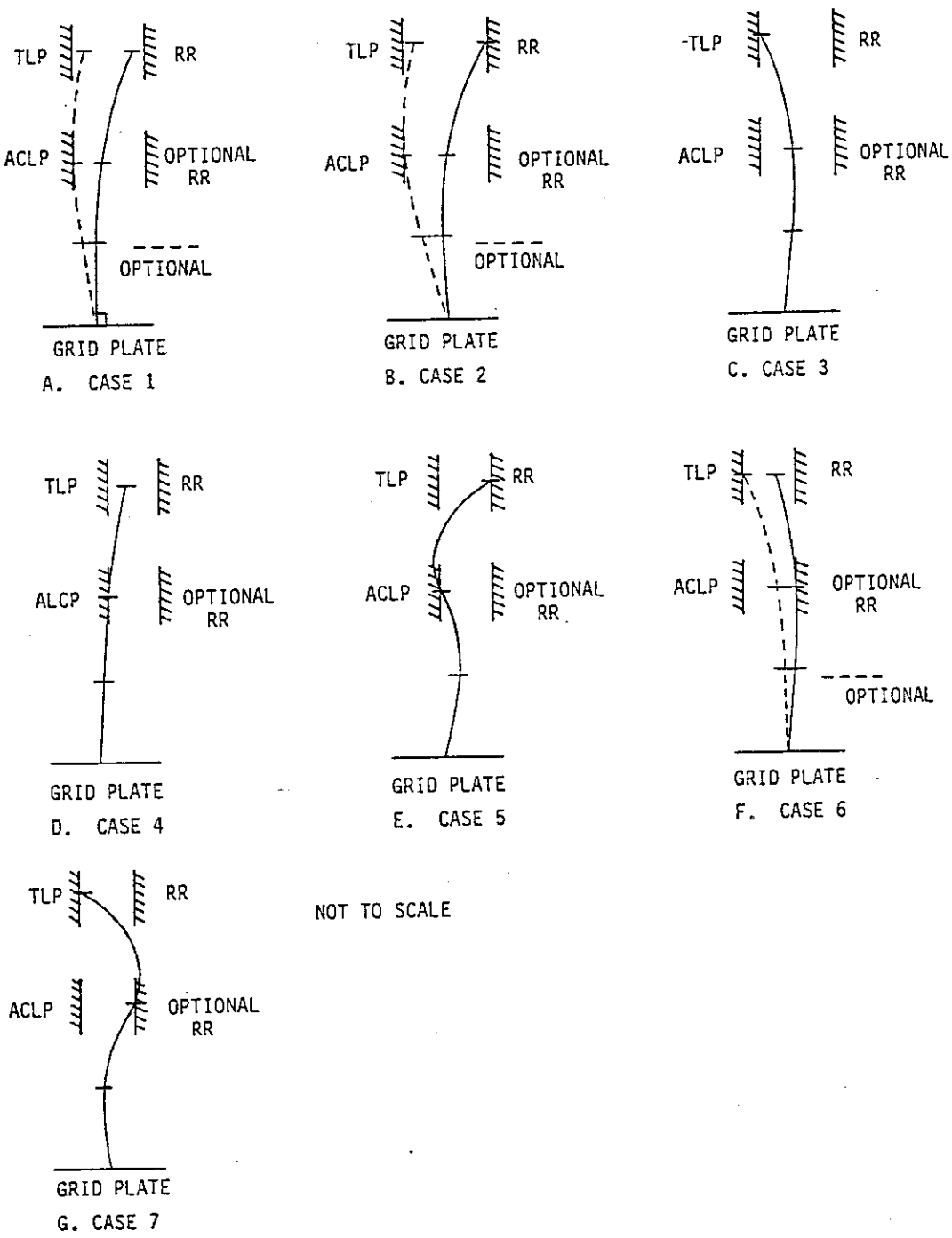

Fig. 7. Subassembly Shapes for Various Core Loading States With the Subassembly Free to Tilt at the Grid Plate

An option is available for this case which accounts for the behavior of the outer assemblies. For cases where the outer assemblies have large radial temperature gradients or irradiation effects causing outward bending at the top, the single subassembly will be pushed inward until it contacts either the compacted ACLP or TLP region. This is also shown in Fig. 7a. The equation defining this case is

$$y(x) = \frac{M_1}{6EI(a-x_1)} (x-x_1)^3 + S_{GR}x \qquad \text{for } x_1 \le x \le a$$

where

$S_{GR} = (R_1-y_a)/a$

R_1 = equivalent radius of the compacted ACLP region, m

or,

$S_{GR} = (R_2-y_L)/L$

R_2 = equivalent radius of the compacted TLP region, m

depending on which compacted load pad region is contacted.

A similar situation is encountered with inward bending in the outer assemblies. The option in the model will accommodate this situation if the bending stiffness of these assemblies is small compared to the core assemblies, as it is in FFTF.

Case 2: Contact at the Top Restraint Ring Only, Grid Plate/ Subassembly Clearance Not Exceeded

For this case, the thermal bending of the subassembly is sufficient to close the gap between the subassembly TLP and the restraint ring, with the outer assemblies pushed against the restraint ring. The interference at the TLP causes the subassembly to be tilted inward until there is no interference, and there is still clearance at the ACLP, both with the compacted load pad region of the interior subassemblies, and with the restraint ring, if present. This case is shown in Fig. 7b. The equation defining the shape of the core region is as follows:

$$y(x) = \frac{M_1}{6EI(a-x_1)} (x-x_1)^3 + S_{GR}x \qquad \text{for } x_1 \le x \le a$$

$$S_{GR} = (R_3-y_L)/L$$

R_3 = equivalent radius of the top restraint ring boundary, m

For this condition, with the radial temperature gradient as shown in Fig. 2, increase in power results in a decrease in the size of the core, or a positive reactivity feedback. This is an undesirable situation, since the magnitude of this feedback is not necessarily small with respect to the other negative feedbacks.

Case 2 assumes that all of the outer assembly load pads are pushed out at the top against the restraint ring. Given that the single subassembly is free to tilt at the grid plate, any resistance in moving the outer assemblies outward would cause the single assembly to move inward. This core loading configuration is also sensitive to the same phenomena discussed for Case 1. The option is available for pushing the subassembly inward until either the compacted ACLP or TLP region is contacted. The equation for y(x) is unchanged, with S_{GR} as follows:

$$S_{GR} = (R_1-y_a)/a$$

or

$$S_{GR} = (R_2-y_L)/L$$

depending on which compacted load pad region is contacted first.

Case 3: Contact at the TLP Only, Grid Plate/Subassembly Clearances Not Exceeded

The thermal bending of the subassembly is not sufficient to prevent interference with the compacted load pad region at the TLP, but there is clearance with the restraint ring(s) and the compacted load pad region at the ACLP. This case is shown in Fig. 7c. This shape of the core region uses the same equation as Case 2, but with a different value for S_{GR}:

$$S_{GR} = (R_2 - y_L)/L$$

This situation would be expected where the radial thermal gradient in the outer rows of drivers was reversed from that shown in Fig. 2. For this case, increase in power would result in a larger core dimension, and negative reactivity feedback. This subassembly shape could also be obtained if there were irradiation effects which deformed the subassembly inwards, even though the temperature gradient would bend the subassembly outwards. In that case, increase in power reduces the core dimension, with a positive reactivity feedback. This could also happen if the size of the compacted load pad region at the TLP were larger than at the ACLP. This condition is determinate if the subassembly is designed to be vertical at the grid plate, but may not be otherwise as there is room for the subassembly to tilt outwards until another restraint is contacted.

Case 4: Contact at the ACLP Only, Grid Plate/Subassembly Clearances Not Exceeded

This case is similar to Case 3, but the contact is now at the ACLP as shown in Fig. 7d. The equation for the core region is the same, with the following value for S_{GR}:

$$S_{GR} = (R_1 - y_a)/a$$

This condition would usually be caused by the greater expansion of the load pad regions as compared to the grid plate, with the thermal bending being insufficient to clear the compacted load pad region. For this condition, increase in power would increase the load pad dimension of the core, which is a negative reactivity effect, while the increased thermal bending would decrease the dimension of the core, a positive reactivity feedback. Since the thermal bending is usually a smaller effect, typically about 30% - 40% as large as the load pad expansion effect, the reactivity feedback is still negative. Again, this subassembly position is determinate if the outer assemblies act to push the subassembly into this position, or if the subassembly prefers the vertical orientation at the grid plate. Otherwise, there is room for the subassembly to take other positions, with different

reactivity implications. This case is identical to including the option in Case 1, when the compacted ACLP region is contacted first.

Case 5: Contact at the ACLP and the Top Restraint Ring, Grid Plate/Subassembly Clearances Not Exceeded

This is one of the most common core loading conditions expected at nominal steady-state. It is characterized by thermal bending sufficient to close the gap at the TLP with the restraint ring and at the ACLP with the compacted load pad region of the interior subassemblies. This situation was depicted on Fig. 6, and is shown again in Fig. 7e. The equation for defining the core region is:

$$y(x) = \frac{M_1}{6EI(a-x_1)}(x-x_1)^3 - \frac{V_{GR}}{EI}\left(\frac{x^3}{6}\right) - \frac{C_1 x}{EI} \qquad \text{for } x_1 \le x \le a$$

$$\frac{V_{GR}}{EI} = \frac{P}{EI}\left(1 - \frac{a}{L}\right)$$

$$\frac{P}{EI} = \left[\frac{R_1 L}{a} - R_3 + \frac{M_1}{EI}\left[\frac{a^3}{3} - \frac{x_1 a^2}{2} + \frac{x_1^3}{6}\right]\left(\frac{L}{a} - 1\right) / (a-x_1)\right.$$

$$\left. + \frac{M_2}{EI}\frac{(L-a)^2}{2}\right] / \left[(a^3 - 2a^2L + aL^2)/3\right]$$

$$\frac{C_1}{EI} = \frac{C_3}{EI} + \frac{M_1}{EI}\left(\frac{x_1^2}{2(a-x_1)}\right)$$

$$\frac{C_3}{EI} = -\frac{R_1}{a} + \frac{M_1}{EI}\left[\frac{a^2}{6} - \frac{x_1 a}{2} - \frac{x_1^3}{6a}\right] / (a-x_1) - \frac{V_{GR}}{EI}\left(\frac{a^2}{6}\right)$$

With the radial temperature gradient causing outward bending of the subassembly, the subassembly position is uniquely defined given that the outer subassemblies either bend in the same outward direction, or have low stiffness

relative to the core assemblies. This results in the largest negative reactivity feedback from increases in power, with both the thermal expansion of the ACLP region and the thermal bending contributing to the negative reactivity feedback. Generally, it is about 30% greater than that from thermal expansion of the load pad region alone. This is one of the preferred conditions for the reactor at nominal full power and full flow.

Case 6: Contact at Above-Core Restraint Ring Only, Grid Plate/ Subassembly Clearances Not Exceeded

This case only applies to reactors which have a restraint ring at the ACLP elevation, such as FFTF. The thermal bending of the subassembly is sufficient to contact the above-core restraint ring through the outer assemblies, but not sufficient to contact at the top. This condition is shown in Fig. 7f, with the shape of the core region given by the equation used for Cases 2-4, with the following value for S_{GR}:

$$S_{GR} = (R_4 - y_a)/a$$

R_4 = equivalent radius of the above-core restraint ring boundary, m

This case is similar to Case 2, 3, and 4 and is subject to the same comments. The subassembly position is not uniquely determined for this case unless the subassembly is designed to be vertical at the grid plate.

The option of pushing the single subassembly inwards until either of the compacted load pad regions is contacted is available for this case. The equation for this case is the same as for Cases 1 and 2, with the same options for S_{GR}:

$$S_{GR} = (R_1 - y_a)/a$$

or

$$S_{GR} = (R_2 - y_L)/L$$

depending on which load pad region is contacted first.

Case 7: Contact at the TLP and the Above-Core Restraint Ring, Grid Plate/Subassembly Clearances Not Exceeded

This case only applies to reactors which have a restraint ring at the ACLP elevation, such as FFTF. In this situation, the outward bending of the subassembly is not sufficient to prevent interference at the compacted TLP region when the above-core restraint ring pushes in on the subassembly, or there is substantial inward bending at the top. This case is shown in Fig. 7g, with the shape of the core region defined by the same equation used for Case 5, but with R_4 replacing R_1 and with R_2 replacing R_3. This case is determinate, but the reactivity implications depend on the relative magnitudes of the thermal expansion and the thermal bending, and could result in positive feedback, possibly of large magnitude.

Case 8: Contact at the Top Restraint Ring Only, No Clearance Remaining at the Grid Plate

This case is similar to Case 2, but with the available clearance for tilting the subassembly at the grid plate exceeded. This changes the boundary condition at the grid from one which provides a force in the radial direction to one which provides a force and a moment, with a prescribed maximum tilt from the vertical at the grid. The input data affecting this case have already been listed in Table 1, where the maximum slope from the vertical is specified. An example of this case is shown in Fig. 8a, with the equations for the core region as follows:

$$y(x) = \frac{M_1}{6EI(a-x_1)}(x - x_1)^3 + xS_{GRMAX} - \frac{V_{GR}}{EI}\left(\frac{x^3}{6}\right) - \frac{M_{GR}}{EI}\left(\frac{x^2}{2}\right) \quad \text{for } x_1 \le x \le a$$

$$\frac{M_{GR}}{EI} = -\frac{V_{GR}}{EI} L$$

$$\frac{V_{GR}}{EI} = \frac{3R_3}{L^3} - \frac{M_1}{EI}\left[3(a-x_1)(L-a)+(a-x_1)^2\right]/2L^3 - \frac{M_2}{EI}\left[3(L-a)^2\right]/2L^3 - 3S_{GRMAX}/L^2$$

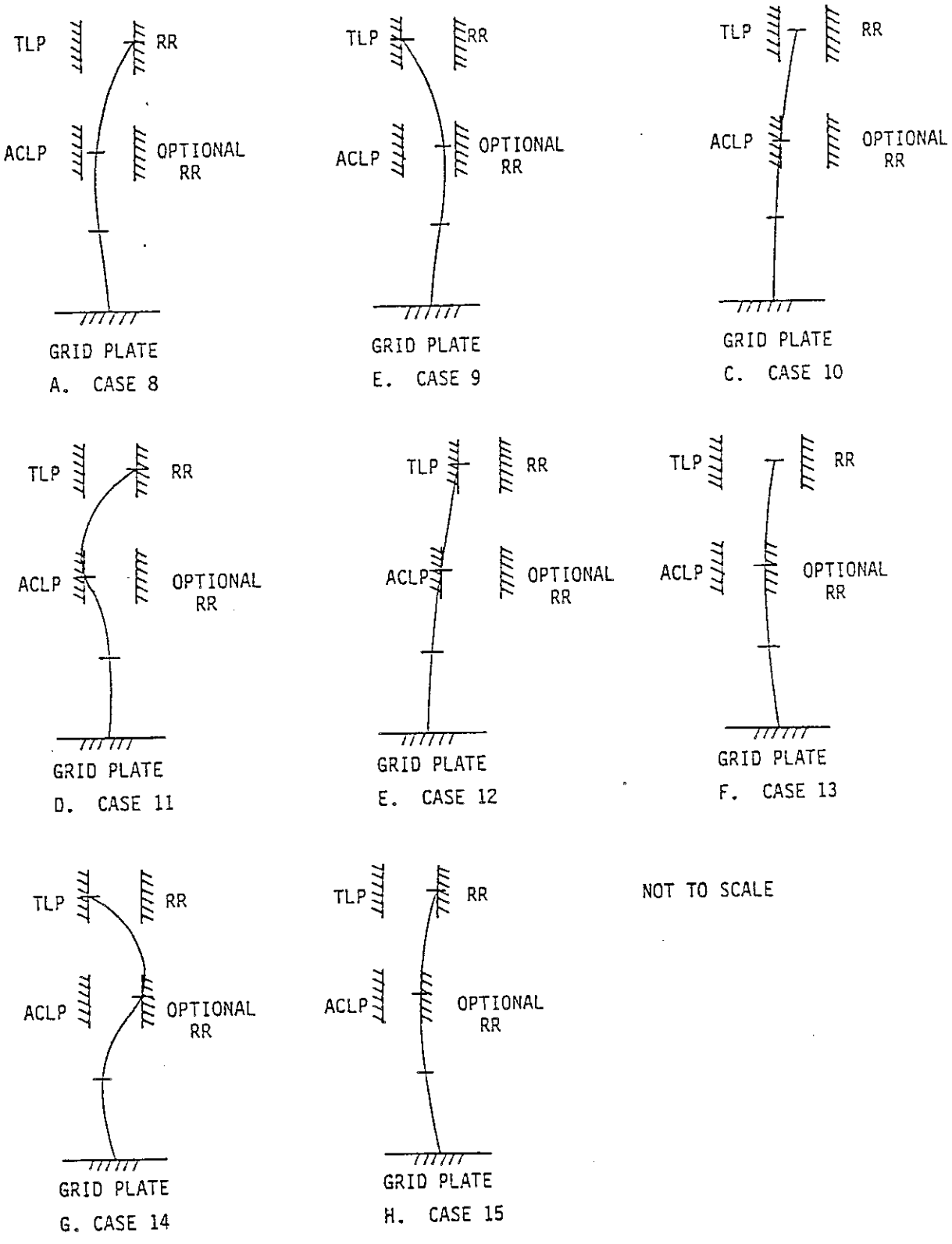

Fig. 8. Subassembly Shapes for Various Core Loading States With the Subassembly Fixed at the Grid Plate

For a radial temperature gradient which causes the subassembly to bend outward, as shown in Fig. 2, increase in power results in a positive reactivity feedback due to the increased bending. Since there is no clearance remaining at the grid plate, this subassembly configuration is determinate, as opposed to Case 2 which is not, in general.

Case 9: Contact at the TLP Only, No Clearance Remaining at the Grid Plate

This case is similar to Case 3, but with any clearance at the grid plate for tilting the subassembly taken up. The change in boundary condition is the same as for Case 8. An example of a possible core shape is indicated on Fig. 8b, with the same equation used for calculating the shape in the core region as in Case 8, but with R_2 replacing R_3.

Figure 8b shows this case for a subassembly with a radial temperature gradient which bends the subassembly inward at the top. This case could also occur if the compacted TLP region were much larger than the equivalent radius at the grid plate. The amount and the sign of the reactivity feedback from an increase in power would depend on the magnitude of the radial temperature gradient. As in Case 8, this subassembly position is determinate.

Case 10: Contact at the ACLP Only, No Clearance Remaining at the Grid Plate

This case is similar to Case 9, but with the contact occurring at the ACLP. It is also similar to Case 4 where the subassembly is free to tilt at the grid plate. An example of this case is shown on Fig. 8c. The equation for the shape of the core region is:

$$y(x) = \frac{M_1}{6EI(a-x_1)}(x - x_1)^3 + xS_{GRMAX} - \frac{V_{GR}}{EI}\left(\frac{x^3}{6}\right) - \frac{M_{GR}}{EI}\left(\frac{x^2}{2}\right) \text{ for } x_1 \le x \le a$$

$$\frac{M_{GR}}{EI} = -\frac{Pa}{EI}$$

$$\frac{V_{GR}}{EI} = \frac{P}{EI}$$

$$\frac{P}{EI} = \frac{3R_1}{a^3} - \frac{M_1}{EI}\left(\frac{(a-x_1)^2}{2a^3}\right) - 3S_{GRMAX}/a^2$$

As in Case 9, the reactivity feedback from an increase in power depends on the magnitude of the radial temperature gradient, and can be either positive or negative. As for the other cases where there is no clearance remaining at the grid plate, this subasssembly position is determinate.

Case 11: Contact at the ACLP and the Top Restraint Ring, No Clearance Remaining at the Grid Plate

This case is similar to Case 5, with no clearance remaining at the grid plate for tilting of the subassembly. An example of this case is shown on Fig. 8d, with the equation for the core region as follows:

$$y(x) = \frac{M_1}{6EI(a-x_1)}(x - x_1)^3 + xS_{GRMAX} - \frac{V_{GR}}{EI}\left(\frac{x^3}{6}\right) - \frac{M_{GR}}{EI}\left(\frac{x^2}{2}\right) \text{ for } x_1 \le x \le a$$

$$\frac{M_{GR}}{EI} = \frac{P}{EI}(L-a) - \frac{V_{GR}}{EI}L$$

$$\frac{V_{GR}}{EI} = \frac{P}{EI}\left[1 + \frac{a^3}{2L^3} - \frac{3a^2}{2L^2}\right] + \frac{3R_3}{L^3} - \frac{M_1}{EI}[3(a-x_1)(L-a)+(a-x_1)^2]/2L^3$$

$$- \frac{M_2}{EI}[3(L-a)^2]/2L^3 - 3S_{GRMAX}/L^2$$

$$\frac{P}{EI} = \left[R_3\left(\frac{3a^2}{L^2} - \frac{a^3}{L^3}\right)\right]/2 - R_1 - \frac{M_1}{EI}\left[\left(\frac{3a^2}{L^2} - \frac{a^3}{L^3}\right)\frac{(L-a)}{4}\right.$$

$$+\left(\frac{a^2}{4L^2} - \frac{a^3}{12L^3} - \frac{1}{6}\right)(a-x_1)\Bigg] \quad (a-x_1) - \frac{M_2}{EI}\left(\frac{3a^2}{L^2} - \frac{a^3}{L^3}\right)\frac{(L-a)^2}{4}$$

$$+ S_{GRMAX}\left(a + \frac{a^3}{2L^2} - \frac{3a^2}{2L}\right)\Bigg]/a^3\left[\frac{a^3}{12L^3} - \frac{a^2}{2L^2} + \frac{3a}{4L} - \frac{1}{3}\right]$$

The reactivity feedback with an increase in power for this example is negative, and probably substantial, although not as large as would occur with the subasssembly loading represented by Case 5.

Case 12: Contact at the ACLP and the TLP,
No Clearance Remaining at the Grid Plate

For this case, the load pad regions in the interior of the core have expanded sufficiently to push the subassembly out so that there was no clearance remaining at the grid plate/subassembly connection. An example of this loading condition is shown in Fig. 8e, with the shape of the core region defined by the the same equations used for Case 11, but with R_2 replacing R_3 in the expressions for V_{GR}/EI and P/EI. This case would probably result in negative reactivity feedback in response to a power increase, although not as large as would be obtained with Case 5 or 11.

Case 13: Contact at the Above-Core Restraint Ring Only,
No Clearance Remaining at the Grid Plate

This case would apply only to those designs which have an above-core restraint ring, such as FFTF. The configuration is similar to Case 6, except that there is no clearance at the grid plate/subassembly connection. The subassembly shape is shown in Fig. 8f, according to the same equation for the core region as used for Case 10 with R_4 replacing R_1. As in Cases 8-12, the subassembly position in this case is also determinate.

Case 14: Contact at the TLP and the Above-Core Restraint Ring, No Clearance Remaining at the Grid Plate

This case only applies to those reactors which have an above-core restraint ring. This case is shown in Fig. 8g, with the shape of the core region given by the same equation as used for Case 11, with R_2 replacing R_3 and R_4 replacing R_1. This case is most likely to occur with inward thermal bending of the subassembly. In either case, positive reactivity should result from an increase in power.

Case 15: Contact at Both Restraint Rings, No Clearance Remaining at the Grid Plate

This case only applies to those reactors which have an above-core restraint ring. This case is shown in Fig. 8h, with the shape of the core region given by the equation used for Case 11 and with R_4 replacing R_1. If this case occurred with outward thermal bending of the subassembly, and expansion of the grid plate, an increase in power would produce positive reactivity feedback for this condition.

4. Steady-State and Transient Calculations

The appropriate subassembly shape is determined as part of the steady-state calculations and the axial profile is saved as the reference core shape for the calculation. During the transient, this reference shape is used for comparison with the results obtained as the transient progresses. The comparison allows the calculation of the changes in core radius for every axial location in the core.

The calculation of the core shape during the transient follows the same algorithm as the steady-state initialization. It is performed at every step in the transient. The logic allows the smooth transition from one core loading state to another, with a continuity in the magnitude of the reactivity feedback, but not necessarily in the rate of change of the feedback with time. The particular core loading that is being calculated is indicated in the printout according to Table 2.

Table 2. Model Designation for Core Shapes Calculated During the Steady-State and the Transient

Case		Model Description	
		Steady-State	Transient
Grid plate/subassembly nozzle clearance not exceeded			
1.	No contact at ACLP, TLP, or RRs	1.0	21.0
2.	Contact at top RR only	2.0	22.0
3.	Contact at TLP only	3.0	23.0
4.	Contact at ACLP only	4.0	24.0
5.	Contact at ACLP and top RR	5.0	25.0
6.	Contact at above-core RR only	6.0	26.0
7.	Contact at TLP and above-core RR	7.0	27.0
No clearance remaining at the grid plate			
8.	Contact at top RR only	8.0	28.0
9.	Contact at TLP only	9.0	29.0
10.	Contact at ACLP only	10.0	30.0
11.	Contact at ACLP and top RR	11.0	31.0
12.	Contact at ACLP and TLP	12.0	32.0
13.	Contact at above-core RR only	13.0	33.0
14.	Contact at TLP and above-core RR	14.0	34.0
15.	Contact at both RRs	15.0	35.0

The first step for each transient time step is to update the sizes of all of the structural regions according to the temperature field occuring at that time in the transient. This includes the grid plate, the compacted load pad regions and the restraint ring(s). The thermal bending moment is modified based on the core temperature rise at that time in the transient in proportion to the steady-state temperature rise. The irradiation bending moment is not changed, since irradiation effects are expected to occur over a much longer period of time.

The other change which may occur during a transient involves the temperature of the load pad regions. At steady-state, this temperature is 75% of the average core temperature rise. However, as experiments and calculations with COBRA-WC [14] and SUPERENERGY-2 demonstrate, the fraction changes when the flow through the subassembly approaches natural circulation levels. This causes the temperature profile across the subassembly to flatten, with the flow in the edge channels being comparable to the flow in the interior of the subassembly. This causes the load pad temperature to approach 100% of the average core temperature rise, so that the load pad will have the same temperature as the coolant. This effect begins below approximately 5% of normal flow. The functional form in the model was selected to duplicate the COBRA-WC load pad temperature calculations during a loss-of-flow transient.

Using this updated information, a shape for the core region is calculated. Given this core shape, and the original shape at nominal steady-state conditions, the displacement of each axial node in the core region is calculated. Once this displacement profile is obtained, the reactivity worth curve for radial core expansion is used to determine the change in the core reactivity from this effect.

5. Reactivity Worth Curve

The reactivity worth curve for radial core expansion is obtained from the worth of a uniform dilation of the core. The uniform dilation value is obtained by increasing the subassembly pitch in the neutronics calculations, and determining the change in reactivity. It is equivalent to an expansion of the grid plate with all of the subassemblies straight and vertical at all times. The calculation is typically performed at a constant and uniform temperature. For use in this model the uniform dilation value is distributed

among the axial nodes according to the axial power shape of the reactor [15]. This distribution is maintained for the duration of the transient.

The use of the uniform dilation worth, suitably distributed among the axial nodes, implies that the fuel material in each axial node is distributed in proportion to its distance from the core centerline. Therefore, while the single subassembly model only calculates a shape for one subassembly representative of a particular row, the subassemblies in the other rows are also displaced in proportion to their distance from the core centerline. This applies to the assemblies in the interior regions and to those exterior to the row represented by the single subassembly model. When the displacement of each axial node has been determined, as described in the previous section, this is used with the displacement worth for each node, and the total reactivity change is the sum over all of the axial nodes. Since all of the steps in the process involve algebraic equations and simple arithmetic operations, this process is used for each step in the transient, and the reactivity change from changes in core shape is followed in detail at every step of the transient.

C. Additional Modelling Options

In addition to the basic modelling information reviewed in Section IV-B, options which are especially pertinent to the modelling of FFTF have been included in the model. These additions may also be important for the representation of advanced LMRs. The additional information can be divided into three sections covering modelling options.

1. Residual Clearance in the Core Interior

One addition contained in the input data reviewed in Table 1 is for the non-ideal compaction of the load pad regions. This input is included based on the results of the full scale subassembly compaction tests, which showed that even when all of the subassembly load pads had the same size, efforts to push them perfectly together were unsuccessful, and a residual gap remained [16]. This gap was randomly distributed throughout the core.

Based on the expected subassembly deflections, it was anticipated that this feature would not have any impact on the modelling of advanced LMR designs using a limited free-bow core restraint design and one restraint ring,

since it only slightly changed the starting dimensions of the core region. However, in FFTF, the presence of the restraint ring at the above-core load pad elevation could make this change significant. The restraint ring limits the thermal expansion of the above-core load pad region, and any residual clearance in the interior of the core at the start of the transient leaves less room for thermal expansion of the above-core load pads as a result of conditions occurring during the transient.

2. Additional Clearance at the Top Load Pads

Another feature which is included for modelling the FFTF reactor involved the design of the top load pads. In FFTF, these are not solidly attached to the subassembly, but "float" on the subassembly hexcan. This provides additional clearance between the subassembly and the restraint provided by the load pads out to the restraint ring. This design feature has not been repeated in other reactors, as more experience has been gained with core design and advanced alloys for core materials.

3. Optional Behavior of the Exterior Subassemblies

This option is included to account for the possibility that the outer assemblies may impose an additional boundary condition on the single subassembly usually respresenting the outermost row of drivers. In particular, there may be sizeable temperature gradients without the accompanying displacement worth, there may be irradiation effects resulting in sizeable deflections, or there may be reverse deflections. All of these act to push the core together when the behavior of the single subassembly may not be sufficient to do so. These effects are discussed in Section IV-B-3 for cases where they have an impact on the core size.

This option provides for the subassembly to take the position which would give the smallest dimension of the core. While the subassemblies are pushed together, rather than assuming that a subassembly would remain vertical at the grid plate, there is no force provided to elastically deform the single subassembly. This option only specifies a particular position for the subassembly, but does not alter the shape determined by the thermal gradients. For the subassemblies which bend outward at the top, this usually amounts to pushing the ACLP against the compacted load pad region for all but the lowest

powers, where the straightening of the subassembly may cause the TLP to make contact first.

This option would generally apply to those designs where the outer assemblies are of much lower bending stiffness than the core assemblies, as in FFTF. It would also apply in those cases where the subassemblies are pushed together at the ACLP, regardless of the stiffness. There is concern that some scenarios involving reverse bending with B_4C shield assemblies will complicate this approach [17]. However, there are several disadvantages with such a situation which would make this a loading condition to be avoided by design, especially concerning the ability to define the core geometry with certainty and the magnitude of the intersubassembly loads involved. For these reasons, the approach of having the single assembly pushed inward without any force has been adopted. If subsequent designs require a change in this option, an extension in the model can be made.

V. SASSYS MODELLING FOR FFTF

The system model for FFTF has been developed for validating the SASSYS code and for analyzing the safety characteristics of FFTF as the change is made to metallic fuel [6,18]. The current SASSYS/SAS4A model of the radial core expansion in FFTF includes all of the features described in the previous section, along with additional modelling covering other structures in the core region. In the following, the details of the modelling for the oxide core in FFTF are reviewed, and the present estimate of the metallic fuel core is also covered.

A. Modelling the FFTF Core Restraint

The core restraint design for FFTF [19] is shown schematically in Figure 4. The top restraint ring is composed of 6 yoke pieces. These yoke pieces form a ring around the periphery of the reflector load pads, but there are small gaps between each of the yoke pieces. The continuous solid boundary is provided by the core barrel through the upper arm of the core restraint system module. The yoke pieces are each mounted on the upper arm of the restraint system module. The module is solidly connected to the core barrel. For this restraint, the radial location of the yoke pieces is controlled by the core barrel and module arm dimensions. This section of the core restraint is at a temperature only slightly higher than the core inlet temperature, according to Westinghouse Hanford Company (WHC) [20]. The yoke pieces themselves are at a much higher fraction of the core temperature rise at steady-state, but the change in their radial dimension is very small compared to the movement of the core barrel and module arm.

The above-core restraint ring is also composed of 6 yoke pieces which mate with the reflector load pads at room temperature. These pieces are connected to a ring, the static ring, which is supported by the inner shield assemblies. The static ring is made of several pieces connected together to form a continuous ring around the core. The static ring is only loosely connected to the lower arm of the restraint system module. In this way, the above-core load pad region has a maximum size determined by the yoke pieces and the static ring, but the static ring is free to move approximately 7.6 mm (0.30 in.) in the radial direction. This maintains core geometry during a seismic event, while the allowable motion reduces the loads associated with

such an event. The maximum allowable size of the core is determined by the dimension of the static ring. The static ring temperature is a significant fraction of the core temperature rise, apparently about 41% [20]. This provides much greater radial movement of the yoke pieces at the above-core load pad elevation than at the top load pad elevation during the rise to power. These design and construction differences between the restraint at the above-core and top load pad elevations also cause the restraint at these two elevations to behave quite differently during the longer term of protected and unprotected accidents. In comparison with the earlier study [4], these differences provide a much greater clearance between the above-core load pads and the yoke pieces at nominal steady-state conditions. There was no significant change at the top load pad elevation.

The nominal dimensions for room temperature conditions are listed in Table 3. The size of the yoke pieces is estimated from the effective radius of the yoke face to its connection to either the static ring (ACLP) or the module upper arm (TLP). These dimensions, and the temperatures at nominal steady-state conditions, are consistent with the information provided by WHC [20]. The dimensions are appropriate for the current oxide fuel core with 316 SS ducts. The clearances listed are between the perfectly compacted load pad regions and the respective yoke pieces. Any non-ideal arrangement of the load pad regions which results in gaps in the interior of the core region will be reflected as a reduction in this clearance during the calculation. The dimensions and temperatures for these subassembly designs are converted into the appropriate input variables for SASSYS and SAS4A as listed in Table 4. Due to the modelling of the reactor core and the nature of the FFTF core restraint system, several minor additions to the coding were needed. These changes are listed in Table 5, and contain the calculations for the core barrel and the module arm.

B. Steady-State Model Validation in FFTF

The reactivity changes associated with changes in power-to-flow ratio have been deduced from experimental measurements in FFTF. These results have been used to validate the current approach to calculating radial core expansion reactivity feedback. Due to the nature of the design, and the irradia-

Table 3. Nominal FFTF Core Restraint System Dimensions for the Current Oxide Fuel Core

Component	Dimension at Ref. Temp.	Temperature at Nominal Steady State
Above-Core Load Pad (ACLP)	1.1976 x 10-1 m (4.715 in.)	759.4 K (a) (907 F)
Top Load Pad (TLP)	1.1976 x 10-1 m (4.715 in.)	759.4 K (a) (907 F)
Subassembly Pitch at the Grid Plate	1.2014 x 10-1 m (4.730 in.)	633.2 K (b) (680 F)
Clearance between Load Pads and Yoke at ACLP	3.1496 x 10-3 m (c) (0.124 in.)	
Clearance between Load Pads and Yoke at TLP	5.6642 x 10-3 m (c) (0.223 in.)	
Reflector Load Pads	1.1976 x 10-1 m (4.715 in.)	674.8 K (d) (755 F)
Static Ring Radius (ACLP)	1.1430 m (45.0 in.)	708.2 K (e) (815 F)
Core Barrel Radius	1.8034 m (71.0 in.)	648.7 K (f) (708 F)
Lower Yoke (ACLP)	(g)	708.2 K (h) (815 F)
Upper Module Arm and Yoke (TLP)	(g)	649.8 K (h) (710 F)
Above-Core Load Pad Elevation	2.1527 m (84.8 in.)	
Top Load Pad Elevation	3.3337 m (131.2 in.)	

Notes:
(a) Subassembly load pad temperatures are assumed to be 75% of the core temperature rise for flow rates over 5% of nominal.
(b) Core support plate, or grid plate, is assumed to be at the nominal inlet temperature at steady-state.
(c) Average dimensions from the reactor as built [20].
(d) Reflector load pad temperatures are set to 755 F [20].
(e) Static ring temperature is set to 815 F [20].
(f) Core barrel temperature is set to 708 F [20].
(g) Code calculates these dimensions at the reference temperature of 80 F.
(h) Yoke temperatures are assumed to be the same as either the static ring temperature (ACLP) or the upper module arm temperature (TLP).

Table 4. SASSYS and SAS4A Input for the Core Restraint Model of FFTF

Variable	Location (Block, #)	Oxide Core 316 SS Duct and Load Pads	Metallic Core HT-9 Duct and 316 Load Pads	Metallic Core HT-9 Duct and Load Pads
IRADEX	1,36	- 4	- 4	- 4
NSUBTC	1,51	91	91	91
MTGRD	1,52	1	1	1
MTACLP	1,53	1	1	2
MTTLP	1,54	1	1	2
NSUBTR	1,59	199	199	199
NRRNGS	1,60	2	2	2
MTRRAC	1,61	1	1	1
MTRRT	1,62	1	1	1
MTRFAC	1,63	1	1	1
MTRFT	1,64	1	1	1
IROPT	1,65	1	1	1
SLLMAX	12,408	1.00000D+00	1.00000D+00	1.00000D+00
PITCHG	12,409	1.20142D-01	1.20142D-01	1.20142D-01
PITCHA	12,410	1.19761D-01	1.19761D-01	1.19888D-01
PITCHT	12,411	1.19761D-01	1.19761D-01	1.19888D-01
RDEXCF	12,412	-3.18900D+02	-1.59100D+02	-1.59100D+02
TLPRRC	12,413	5.66421D-03	5.66421D-03	5.02813D-03
BNDMM1	12,414	1.40000D-03	1.00000D-03	1.00000D-03
BNDMM2	12,415	1.40000D-03	1.00000D-03	1.00000D-03
DFLTCS	12,419	2.55816D-03	0.0	0.0
DFLTSS	12,420	9.80323D-03	0.0	0.0
ACLPRC	12,421	3.14961D-03	3.14961D-03	2.51353D-03
FCDTR1	12,422	4.09000D-01	4.09000D-01	4.09000D-01
FCDTR2	12,423	1.02000D-01	1.02000D-01	1.02000D-01
FCDTRF	12,424	2.50000D-01	3.50000D-01	3.50000D-01
DRCOLL	12,425	3.30200D-03	0.0	0.0
CRSAC	12,426	6.35000D-04	6.35000D-04	6.35000D-04
RR1TC	12,427	2.00000D+02	2.00000D+02	2.00000D+02
RR2TC	12,428	5.00000D+02	5.00000D+02	5.00000D+02

Table 5. Code Modifications for Modelling FFTF

```
*SUBS REXD..74
      JCTLP=MZC-6
*SUBS REXD..78
      NNDUCS=MZC-5-JSTRDX
*SUBS REXD..81
     & (JSTRDX+K-1))/(ZCOOL(MZC-5)-ZCOOL(JSTRDX))
*SUBS REXD.153
      PITCHR=1.19761D-01
      ARCORE=SQRT(3.0D0)*(NSUBTC*PITCHA*PITCHA+(NSUBTR-
     &       NSUBTC)*PITCHR*PITCHR)/2.0D0
*SUBS REXD.155
      ARCORE=SQRT(3.0D0)*(NSUBTC*PITCHT*PITCHT+(NSUBTR-
     &       NSUBTC)*PITCHR*PITCHR)/2.0D0
*INSE REXD.183
C
C     YOKE FACE POSITION AT THE ACLP AT 80 F
      RSTATR=1.143D+00
      YKSTRA=RSTATR-RRNGR1
C
C     FCDTR1 SHOULD BE 0.409 FOR FFTF ACRR
C
      RSTAT=RSTATR*(1.0D0+DELTR1)
      YKSTR=YKSTRA*(1.0D0+DELTR1)
      RRNG1=RSTAT-YKSTR
C
*INSE REXD.192
C     CORE BARREL RADIUS AT 80 F
      RCBARR=1.803D+00
C     MODULE/YOKE DIMENSION AT THE TLP AT 80 F
      YKMTLP=RCBARR-RRNGR2
C
C     FRACTION OF CORE DT FOR CORE BARREL TEMPERATURE
      FCDTCB=0.0954D0
C     CORE BARREL THERMAL TIME CONSTANT
      CB2TC=500.0D0
C     CORE BARREL MATERIAL-STAINLESS STEEL
      MTCB=1
C
C     STEADY-STATE CORE BARREL RADIUS
C
      TCBRL=TINTSS+FCDTCB*(TTLPSS-TKEL-TINTSS)
      TSCBN2=TCBRL
      TRCBN2=TCBRL
      DELTCB=THRMEX(MTCB,TCBRL)*(TCBRL+TKEL-TR)
      RCBARS=RCBARR*(1.0D0+DELTCB)
C
C     FCDTR2 SHOULD BE 0.102 FOR FFTF TOP RR
C
      YKMTLS=YKMTLP*(1.0D0+DELTR2)
      RRNG2=RCBARS-YKMTLS
```

Table 5 (Cont'd)

```
C
*SUBS REXD.219
      ZTOP=2.432D0
*SUBS REXD.221
      ZACLP=1.251D0-ZCOOL(1)
*SUBS REXD.225
      R2=RTLP-RGRSS+CRSAC-DRCOLL
*INSE REXD.592
      WRITE (IWRITE,11201) TCBRL,RCBARS,RSTAT,YKSTR,YKMTLS,YKMTLP
11201 FORMAT ('  TCBRL=',1P,D13.6,'  RCBARS=',D13.6,'   RSTAT=',
     & D13.6,'   YKSTR=',D13.6,'  YKMTLS=',D13.6,'  YKMTLP=',D13.6)
*SUBS REXD.635
      JCTLP=MZC-6
*SUBS REXD.639
      NNDUCS=MZC-5-JSTRDX
*SUBS REXD.642
     & JSTRDX+K-1))/(ZCOOL(MZC-5)-ZCOOL(JSTRDX))
*INSE REXD.707
C     FFTF STATIC RING/YOKE DIMENSIONS
C
      RSTATT=RSTATR*(1.0D0+DELTR1)
      YKSTRT=YKSTRA*(1.0D0+DELTR1)
      RRNG1=RSTATT-YKSTRT
C
*INSE REXD.717
C
C     TRANSIENT CORE BARREL DIMENSION
C
      TSCBR2=TTLPAV-TKEL
      TSCBR2=FCDTCB*(TSCBR2-TINTST)+TINTST
      IF(DTIME.GT.(CB2TC*2.0D0)) CB2TC=DTIME/2.0D0
      TCBRL=(TRCBN2*(1.0D0-DTIME/(2.0D0*CB2TC))+DTIME*(TSCBR2+TSCBN2)/(
     & 2.0D0*CB2TC))/(1.0D0+DTIME/(2.0D0*CB2TC))
      TSCBN2=TSCBR2
      TRCBN2=TCBRL
      DELTCB=THRMEX(MTCB,TCBRL)*(TCBRL+TKEL-TR)
      RCBART=RCBARR*(1.0D0+DELTCB)
C
C
C     FFTF TOP MODULE DIMENSION
C
      YKMTLT=YKMTLP*(1.0D0+DELTR2)
      RRNG2=RCBART-YKMTLT
C
*SUBS REXD.734
      R2=RTLP-RGRSS+CRSAC-DRCOLL
*INSE REXD1097
      WRITE (IWRITE,12201) TCBRL,RCBART,RSTATT,YKSTRT,YKMTLT,RRNG2
12201 FORMAT ('  TCBRL=',1P,D13.6,'  RCBART=',D13.6,'  RSTATT=',
     & D13.6,'  YKSTRT=',D13.6,'  YKMTLT=',D13.6,'   RRNG2=',D13.6)
```

tion effects on 316 SS in the core, the reactivity change could not be completely predicted a priori by the model. The main features are calculated correctly, and once the irradiation effects are included, the agreement between the experimental data and the model calculations is within a few percent. For the current oxide design, irradiation effects were included in the form of initially bent subassemblies. The irradiation induced deflection was selected so that there was only bending in the core region, with the regions above and below the core remaining straight. The magnitude of the deflection was chosen for best agreement with the steady-state curve of radial expansion feedback as a function of power-to-flow ratio [21].

This process is demonstrated in Fig. 9. The initial calculations with the radial core expansion reactivity feedback model indicate that there are two core loading states which are possible in the range of power-to-flow ratio from 0.0 to 2.0 using the data in Table 4. These are obtained using the option with the outer assemblies pushing in on the single subassembly. They are equivalent to Cases 4 and 5 described in Section IV-B-3 and are shown in Fig. 10. For the core loading state occurring at low power-to-flow ratios, Case 4, the subassembly ACLP is pushed inward against the compacted ACLP region by the outer assemblies. As the core outlet temperature increases, with a constant inlet temperature, this allows thermal expansion of the ACLP region to increase the size of core with an associated negative reactivity feedback. However, the increase in the core temperature rise also increases the thermal bending of the subassembly. This acts to reduce the size of the core, but to a lesser degree. The resulting change in reactivity with power-to-flow ratio, i.e., core outlet temperature, is shown on Fig. 9. The slope of the line is not as great as for thermal expansion of the load pad region alone.

For higher power-to-flow ratios, the core loading is represented by Case 5. The subassembly ACLP is pushing against the compacted ACLP region as a result of the TLP pushing outwards against the restraint ring. In this case, an increase in the core temperature rise causes thermal expansion of the load pads and additional thermal bending of the subassembly, as before, but both act to increase the size of the core. This greatly increases the slope of reactivity as a function of the power-to-flow ratio, as shown on Fig. 9. The slope is greater than for load pad thermal expansion alone.

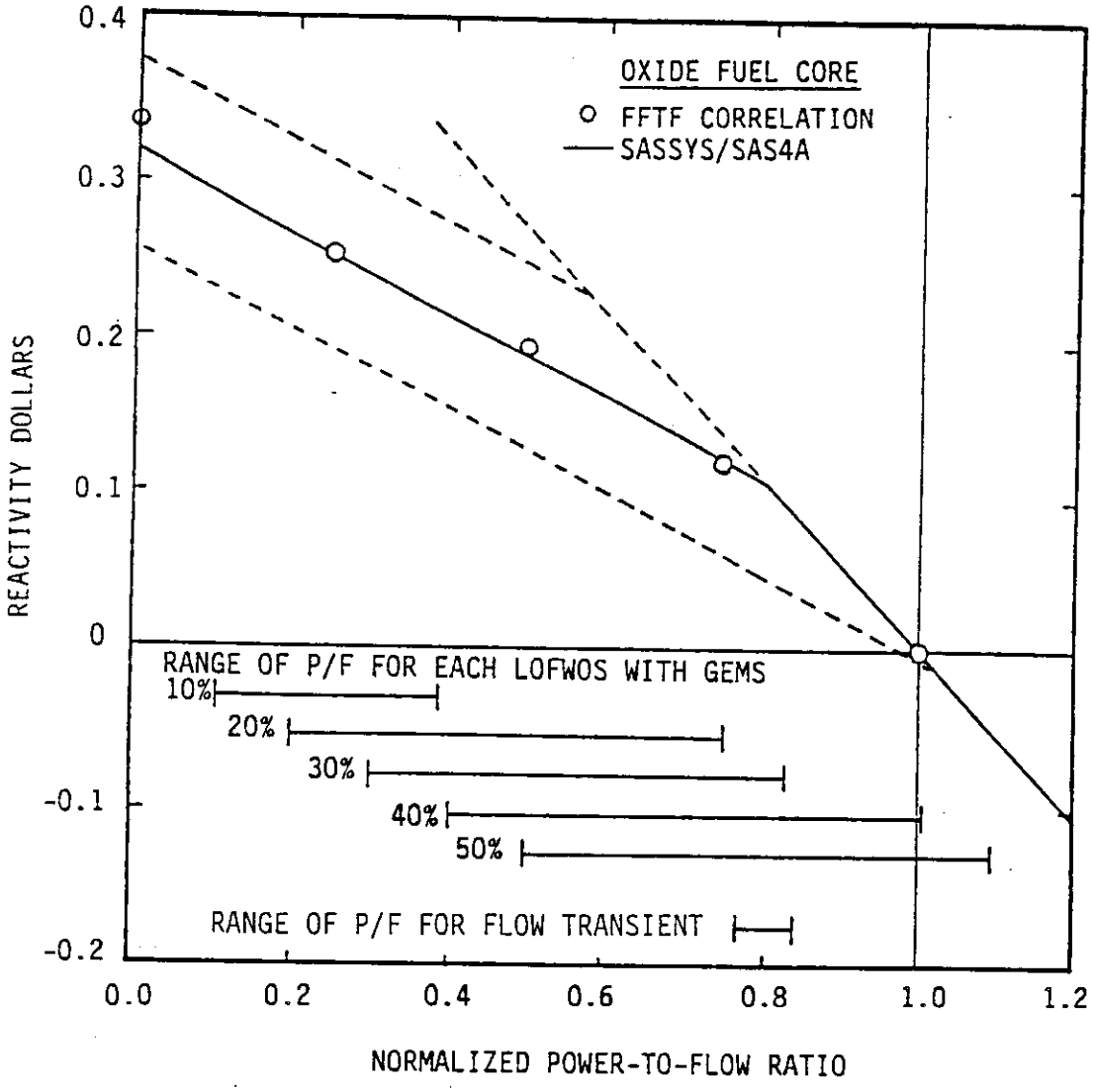

Fig. 9. Reactivity as a Function of Normalized Power-to-Flow Ratio in FFTF

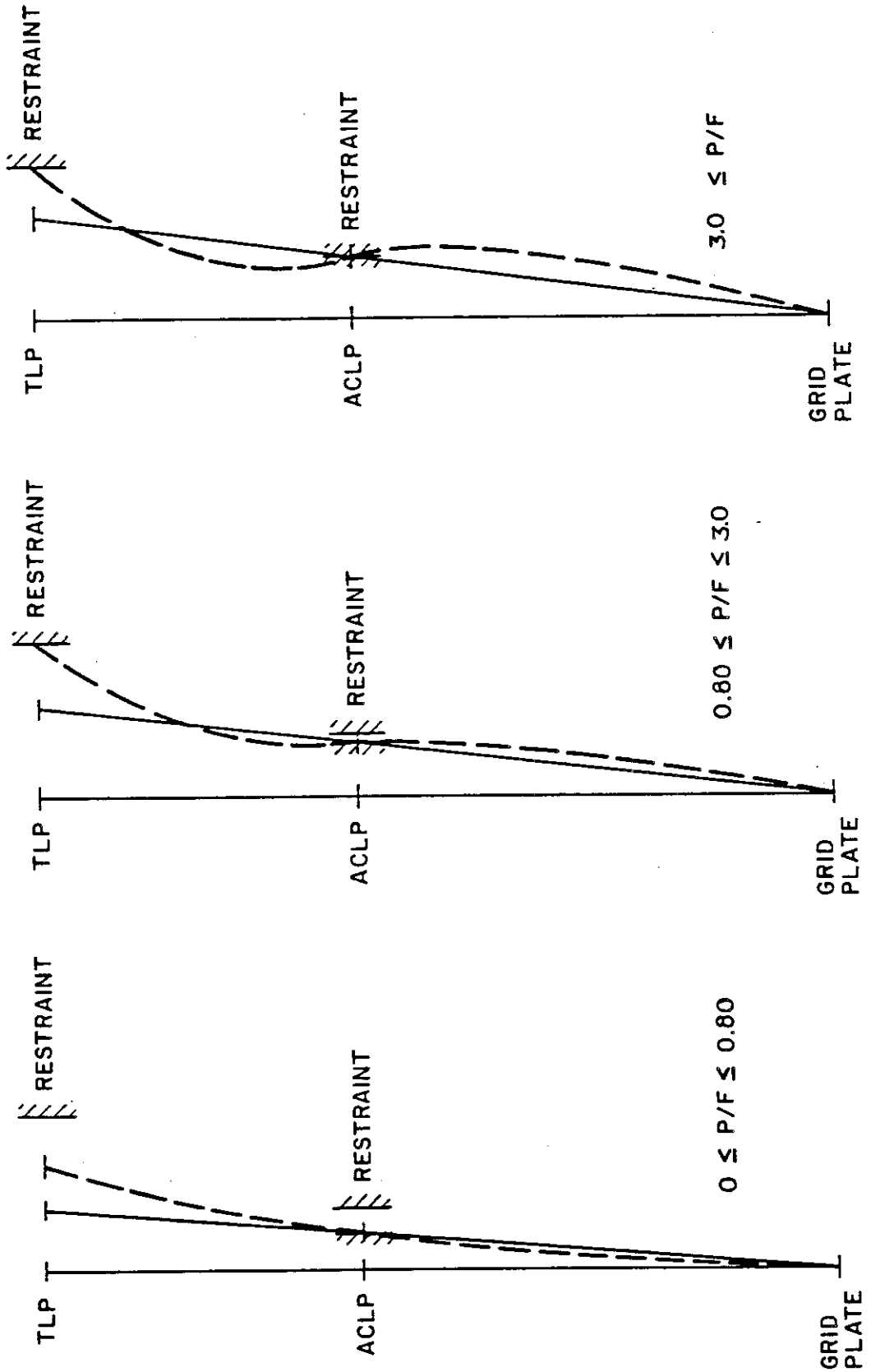

Fig. 10. Subassembly Shapes in FFTF for Several Ranges of Normalized Power-to-Flow Ratio

Due to the large clearances in the FFTF reactor, the transition from Case 4 to Case 5 occurs at a power-to-flow ratio greater than 1.0 if no other effects are considered. However, the power-to-flow ratio where the transition is made from one core loading state to the next can be strongly affected by irradiation effects. For each core loading state, there is a characteristic change in reactivity with power-to-flow ratio, i.e., temperature. The initial calculations are indicated in Fig. 9 by the series of parallel lines. The model correctly calculates the slope of the reactivity vs. power-to-flow ratio lines for both regions. By selecting the irradiation deflection listed in Table 4, the transition from one core loading state to the next occurs at around 0.8, with very good agreement with the experimental data. The amount of irradiation-induced deflection is well within the observed values for driver assemblies in this region of the core.

The steady-state curve also includes values in the range of power-to-flow ratio from 1.0 to 2.0 [21]. These were obtained by WHC using a version of the NUBOW-3D code. These calculations indicated that the above-core load pad region would contact the above-core restraint ring for a power-to-flow ratio only slightly greater than 1.0. This behavior was duplicated with the SASSYS/SAS4A radial core expansion reactivity feedback model by using a large value for the residual clearance in the interior of the core [4]. Several assumptions were also made concerning the core restraint system and the core clearances. These were based on the information available at the time. When more data was obtained [20], these new values were used in the model, as described above. However, the results indicated that the above-core load pads would not contact the above-core restraint ring until a power-to-flow ratio greater than 3.0. This difference has substantial implications for the consequences of unprotected transients where the power-to-flow ratio is significantly greater than 1.0 for extended periods of time. Although this discrepancy between the two estimates cannot be resolved with the steady-state data, some verification is obtained from the transient experiments.

The agreement between the experimental data for power-to-flow ratios of 1.0 or less and the results from the model provide an initial validation for the model in that the behavior of reactivity change as a function of power-to-flow ratio is correctly predicted. The experimental results were only used to establish the proper transition point from one core loading state to the

next. It is not known at this point if the irradiation deflection used is representative of an average of the driver assemblies in the outer row, since such information is not available.

C. Transient Model Validation in FFTF

The radial core expansion reactivity feedback model has also been validated with the results of transient experiments in FFTF [6]. Two representative examples are reviewed in this section. These comparisons not only support the steady-state validation, but also verify that the transient response, with all of the estimates for the associated time constants, is being simulated properly.

1. FFTF GEMs Tests

These tests were unprotected loss-of-flow experiments from reduced power and full flow in FFTF, where several of the radial reflector assemblies were replaced by gas expansion modules (GEMs). The large amount of negative feedback associated with the GEMs was sufficient to prevent coolant boiling in the tests. The net reactivity during the test starting at 50% power and full flow is shown in Fig. 11, along with the SASSYS calculations. While the magnitude of the reactivity is dominated by the GEMs, the variation in net reactivity after approximately 40-50 seconds is controlled by radial core expansion effects. All of the variations are reproduced to within a few percent out to 240 seconds. Since this calculation covers the range of power-to-flow ratio from 0.50 (initial) to 1.1 (peak) which contains the transition from one core loading state to the next, this agreement between model calculations and experimental results provides support for all facets of the model, including the selection of the irradiation-induced deflection, the clearance with the above-core restraint ring, and the transition point. Similar comparisons have been obtained for the entire range of GEMs tests [6].

2. FFTF Flow Transient Experiment

The flow transient experiment in FFTF was a test of the reactor response to a sudden change in flow through the core. The reactor was operating at 75% of nominal power and 86% flow when the flow was decreased 10%. The details of the flow history are contained in Hill [6]. The net reactivity deduced from

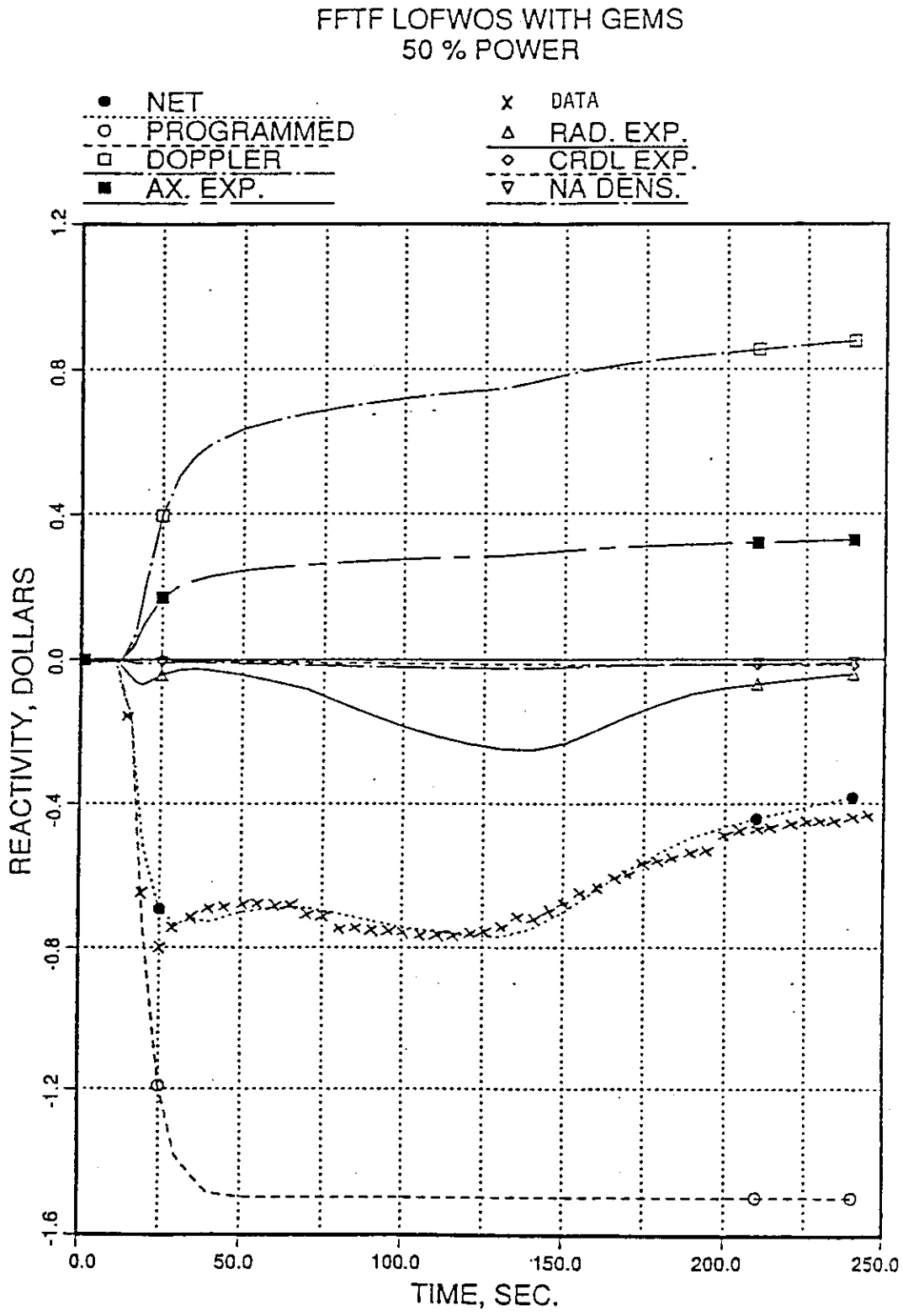

Fig. 11. Calculated and Observed Reactivity as a Function of Time for an Unprotected LOF with GEMs from 50% Power and Nominal Flow

the experiment and the SASSYS calculation are shown in Fig. 12. Again the agreement is to within a few percent until approximately 20-25 seconds, when phenomena occur affecting other assumptions in the SASSYS simulation. This excellent agreement provides further evidence that the radial core expansion effects are being represented accurately, both in magnitude and in timing.

D. Modelling of FFTF with the Proposed Metallic Fuel Design

The excellent agreement with the current oxide core in FFTF justifies the application of the model to the proposed metallic fuel core. There are two designs at present, both with HT-9 for the subassembly hexcans, but one with 316 SS load pads and one with HT-9 load pads. The changes in dimensions for these designs are listed in Table 6. All other dimensions, and modelling of the core restraint system, were unchanged. As listed in Table 4, there is no irradiation-induced deflection in either of these two cases, as HT-9 is expected to be much less susceptible to these effects.

The results for the metallic fuel core using the input data in Table 6 are shown in Figure 13, for HT-9 subassemblies and both 316 SS and HT-9 load pads. In contrast to the results for the oxide core, there are now 3 regions on the curves of reactivity as a function of the normalized power-to-flow ratio. For these calculations, it has been assumed that the subassemblies are initially straight, and that the flat-to-flat temperature difference in the outer row of drivers remains the same for the metallic fuel core. It is also assumed that the new ducted reflectors will provide sufficient bending to push the subassembly load pads together in the core together for even very low power levels. At very low power levels, the top load pad region is compacted with gaps in the above-core load pad region in the interior of the core, as in Case 3. As power increases, there is a slight compaction of the core until there is sufficient thermal bending of the subassemblies to allow contact with both load pad regions. This occurs at a power-to-flow ratio of about 0.33 with 316 SS load pads, and at 0.54 with HT-9 load pads. With further increases in power, the above-core load pad region remains in contact and gaps occur between the top load pads as the top of the subassembly bends outward toward the restraint, as in Case 4. This is the same loading configuration as for the oxide core for a power-to-flow ratio from 0.0 to 0.80. However, for

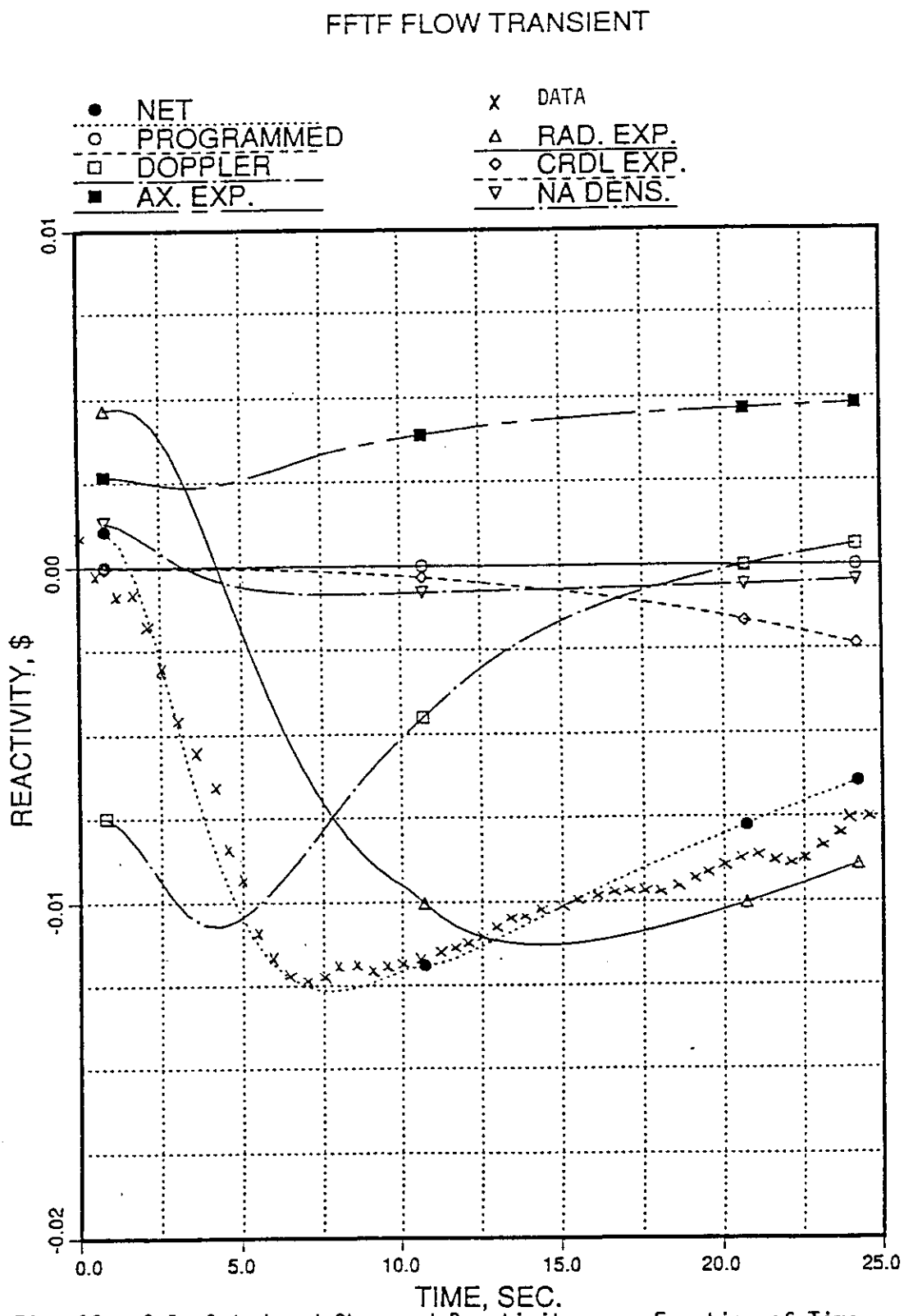

Fig. 12. Calculated and Observed Reactivity as a Function of Time for the FFTF Flow Transient Experiment

Table 6. FFTF Core Subassembly and Restraint System Geometry Changes for the Metallic Core with HT-9 Load Pads

Component	Dimension at Ref. Temp.	Temperature at Nom. S.S.
Above-Core Load Pad (ACLP)	1.1989 x 10-1 m (4.720 in.)	759.4 K (907 F)
Top Load Pad (TLP)	1.1989 x 10-1 m (4.720 in.)	759.4 K (907 F)
Clearance between Load Pads and Yoke at ACLP	2.5135 x 10-3 m (0.099 in.)	
Clearance between Load Pads and Yoke at TLP	5.0281 x 10-3 m (0.198 in.)	

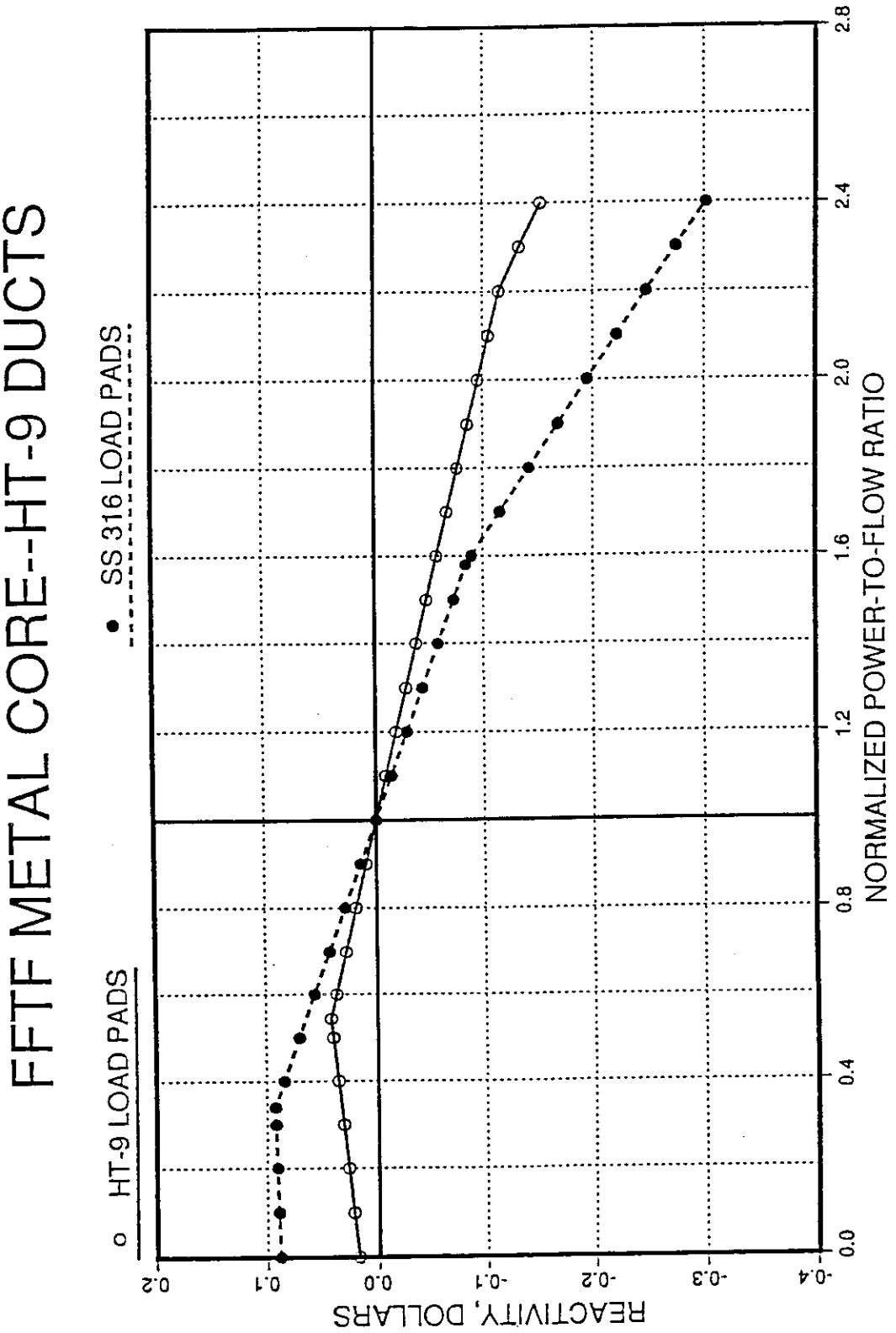

Fig. 13. Reactivity as a Function of Normalized Power-to-Flow Ratio in FFTF for the Proposed Metallic Fuel Core with 316 SS and HT-9 Load Pads

the HT-9 ducts, this region now contains the nominal operating point as well. This difference has an impact on the reactor response to unprotected and protected transients, since the gradient of reactivity change with power-to-flow ratio is substantially reduced with this core loading configuration. At this point, it should be emphasized that these results are obtained assuming that the reflectors will bend enough to push the core together at nominal steady-state conditions. If this doesn't occur, the core could very well be "loose" at nominal conditions, and in situations where the power-to-flow ratio goes above 1.0, the major effect would likely be a tightening of the core, accompanied by positive reactivity feedback until the above-core load pad region was compacted. This would have a substantial impact on the outcome of such a transient.

At power-to-flow ratios much higher than 1.0, that is, 1.58 with 316 SS load pads and 2.20 with HT-9 load pads, the transition is made to the core configuration where the top of the subassembly is pushing out against the restraint, and the above-core load pads are compacted, with both thermal expansion and thermal bending of the subassembly contributing to negative reactivity feedback with increasing power-to-flow ratio. As in the oxide core with 316 SS ducts, this configuration persists to power-to-flow ratios over 3.0 under steady-state conditions before the above-core load pad region contacts the core restraint and further thermal expansion is severely limited by the expansion of the static ring and yoke pieces. In relatively fast transients, such as an unprotected loss-of-flow, the case with HT-9 above-core load pads could contact the restraint at a power-to-flow ratio around 2.0. This is due to the slow response of the restraint to changes in core temperature.

VI. CONCLUSIONS

The development of the detailed radial core expansion reactivity feedback model for SASSYS and SAS4A has been reviewed, with the basic phenomena and the underlying assumptions. The wide range of core loading conditions treated by the model has been discussed in detail, covering all of the anticipated states for a limited free-bow core restraint design. Given the previously existing models for treating this component of the reactivity feedback, this method balances the simplicity of the previous SASSYS/SAS4A model with some of the structural complexity incorporated in NUBOW-3D. The result is a fast-running model, suitable for use in an accident analysis code.

The validation with the FFTF experimental data provides support for both the modelling approach and the assumptions used to simplify the model. Excellent agreement is obtained for both steady-state and transient conditions over a wide range of power and flow. The validity of this approach makes it possible to provide estimates of the behavior of the proposed metallic fuel core in FFTF, so that the response of this system to unprotected accidents can be investigated. The validation of this model can also be transferred to subsequent developments based on the same approach, such as the Single-Assembly and Three-Assembly Models [17], used for analyzing core restraint designs and parameters.

REFERENCES

1. [redacted]

2. [redacted]

3. R. A. Wigeland, "Effect of a Detailed Radial Core Expansion Reactivity Feedback Model on ATWS Calculations Using SASSYS/SAS4A," Trans. Am. Nucl. Soc., 53, p. 303, November 1986.

4. R. A. Wigeland, "Comparison of the SASSYS/SAS4A Radial Core Expansion Reactivity Feedback Model and the Empirical Correlation for the FFTF," Trans. Am. Nucl. Soc., 55, p. 423, November 1987.

5. D. J. Hill and R. A. Wigeland, "Validation of the SASSYS Core Radial Expansion Reactivity Feedback Model," Trans. Am. Nucl. Soc., 56, p. 380, June 1988.

6. D. J. Hill, "SASSYS Validation Studies, " ANL/RAS 88-4, June 1988.

7. T. J. Moran, "Core Restraint Contributions to Radial Expansion Reactivity for the PRISM Cores," ANL-PRISM-19, March 1986.

8. T. J. Moran, "Core Restraint System Design Parameters for the PRISM-87 Core," ANL-PRISM-45, September 1987.

9. S. A. Kamal, "Core Restraint Systems Evaluation for Metal and Oxide SAFR Cores Based on a Bowing Analysis of the Assemblies," ANL-SAFR-9, January 1986.

10. S. A. Kamal, "Assembly Bowing Analysis and Reactivity Feedback of the SAFR Metal Core During Unprotected LOF Transients," ANL-SAFR-41, September 1987.

11. G. A. McLennan, "NUBOW-3D (Inelastic): A FORTRAN Program for the Static Three-Dimensional Analysis of Bowed Reactor Cores Including the Effect of Irradiation Creep and Swelling," ANL-CT-78-19, March 1978.

12. T. J. Moran, "Core Restraint Contributions to Radial Expansion Reactivity," Proc. 1986 Joint ASME/ANS Nuclear Power Conference, Philadelphia, PA, p. 454, July 1986.

13. P. R. Huebotter, Argonne National Laboratory, private communication, June 1981.

14. P. L. Garner, Argonne National Laboratory, private communication, June 1985.

15. H. Khalil, Argonne National Laboratory, private communication, September 1986.

16. W. C. Kinsel, "FTR Core Compaction and Withdrawal Tests," HEDL-TME 73-58, May 1973.

17. T. J. Moran, Argonne National Laboratory, private communication, March 1988.

18. D. J. Hill and F. E. Dunn, Argonne National Laboratory, private communication, April 1987.

19. FFTF System Design Description No. 31, Hanford Engineering Development Laboratory, Revised through February 1984.

20. R. Trenchard, Westinghouse Hanford Company, private communication, January 1988.

21. A. Padilla, Westinghouse Hanford Company, private communication, February 1987.